SPACE COURSE 1993
TU München, Oct. 11-22

SPECTROSCOPIC TECHNIQUES FOR RAM-COMBUSTORS

F. MAYINGER, W. GABLER
Lehrstuhl A für Thermodynamik, Technische Universität München
Arcisstr. 21, 80290 München 2, Germany

and

G. KAPPLER, R. HÖNIG, R. LACHNER
Lehrstuhl für Flugantriebe, Technische Universität München
Arcisstr. 21, 80290 München 2, Germany

Abstract.
Since optical measurement techniques are nonintrusive and very fast, they provide the capability to investigate the mixing process and to investigate the flame structure in highly turbulent flames of ram-combusters without perturbing the flowfield. In this paper the principles of optical arrangements for such experiments are shown, and the techniques of data acquisition and evaluation are discussed. This paper also intends to demonstrate the possibilities of optical measuring techniques for ram-combustors and examples of applications.

1. Introduction and requirements for measurement techniques

Increasing possibilities of computer-aided data processing bestowed a new revival to optical techniques in many areas of mechanical and chemical engineering. For describing complicated phenomena in fluiddynamics or in transfer processes by a computer program global experimental information is not sufficient for developing constitution equations. Furthermore a detailed insight with high local and temporal resolution into thermo- and fluiddynamic situations is necessary. For a better understanding of combustion processes for example it is necessary to know the local concentration and temperature distribution just ahead of the flame and in the ignition zone.

1.1. Adequate temporal and spatial resolution

Since sub- and supersonic reacting flows are highly turbulent, measurement techniques should provide adequate temporal and spatial resolution. The usage of a Nd-YAG laser for laser based scattering measurements like Raman spectroscopy has the following resolutions: temporal resolution (5 ns) and maximum spatial resolution (0.5 mm). Especially Raman spectroscopy is used to measure simultaneously the temperature and the concentrations of all major species (H_2, H_2O, O_2, N_2) in sub- and supersonic flames. By this Raman scattering provides the capability to study turbulence-chemistry interactions in ram-combustors.

1.2. Demand of nonintrusivity for combustion diagnostics

The main feature common to all optical techniques is the non-intrusiveness, meaning that the measurement do not influence the investigated systems in any way as conventional probes often do. Previous experiments in sub- and supersonic combustors, temperature and concentration measurements were made with thermocouples and other intrusive techniques. These conventional probes pertub the flowfield and have poor spatial and temporal resolution that make these measurement systems inadequate for analysis of supersonic flows.

2. Application of measurement techniques

2.1. Analysis of shear- and boundery layer in combusters

Large scaled turbulent structures plays a very important role in chemical mixing of different species in ram combustors, where an important element is the shear layer which separates the fuel jet and the surrounding oxidizer atmosphere. The structure of this mixing layer is influenced by compression/expansion waves and their reflections from the walls. The shadowgraph technique and the holographic interferometry is used to analyse the turbulent structure of shear- and boundery layer in ram combusters (figure 1 and 2).

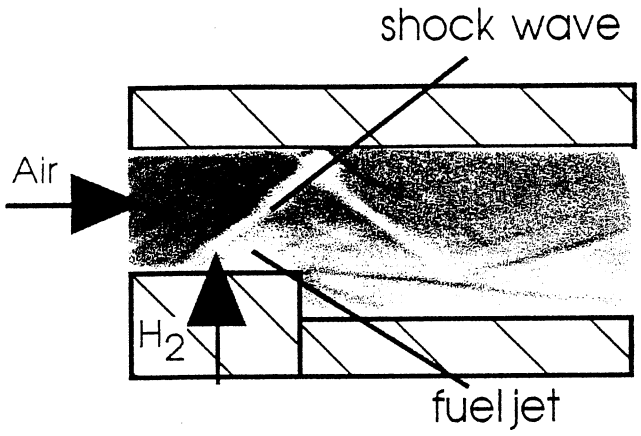

Fig 1: Shadowgraph of a mixing layer with a oblique shock wave at Ma = 2.1

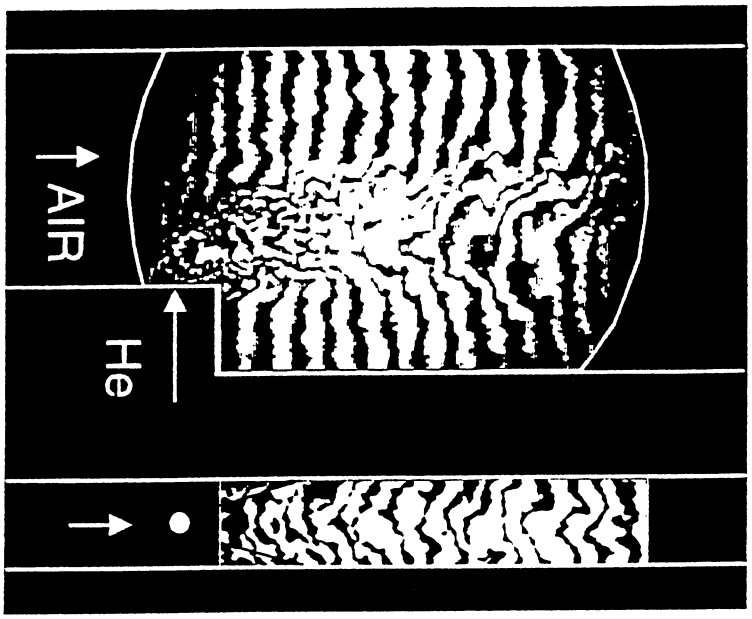

Fig 2: Mixing shear layer in combustion chamber Haibel [1992]

2.2. Investigation of the fuel/air mixing process

Shear layer mixing rates are a major design creterion for sizing combustion chambers. The shadowgraph technique and the holographic interferometrie is used to investigate on line the characteristics of the turbulent transport of mass in the shear layer of combustors. Holographic interferometrie can also provide quantitative measurements in the mixing zone to determine the conzentration profile and the mixing length. More information on these non spectroscopic techniques is provided for example by Mayinger [1993], Panknin [1977] and Haibel [1993]. Furthermore Raman spectroscopy is used to detect the major

species concentration with high temporal and spatial resolution in the mixing area of the combustion chamber. Conzentration measurements in the mixing zone are used to calculate the local state of fuel/air mixing (i.e., mixture fraction) (figure 3 and 4).

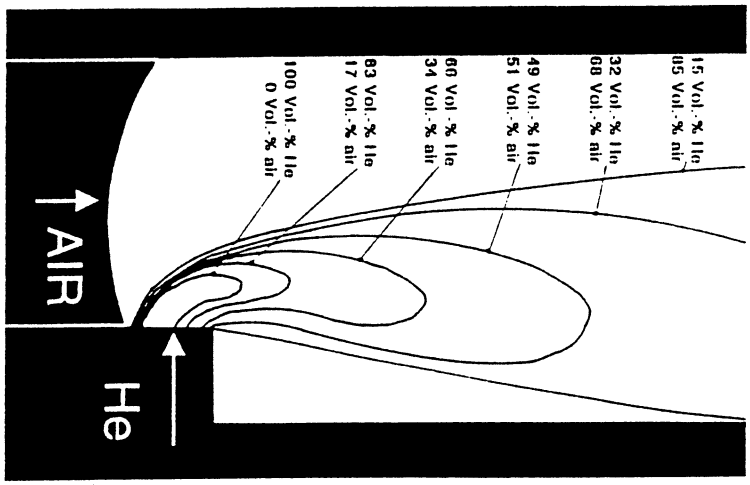

Fig 3: Evaluated concentration profile of the mixing jet (Ma = 0.6) Haibel [1993]

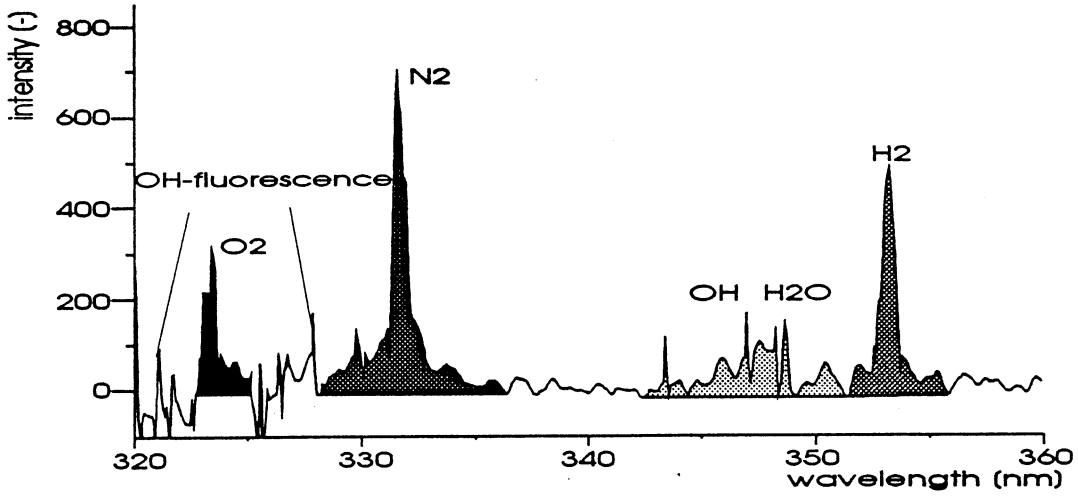

Fig 4: Raman spectrum of major species in a combustion chamber

2.3. Detection of major species concentrations

To achive higher fuel efficiencies and lower emissions of aircraft, it is necessary to understand the turbulence-chemistry interactions in the in the reaction zone. The detection of major species concentrations, especially the measurment of combustion products (H_2O) is used to calculate the combustion efficiency and to study the flame structure. Raman spectroscopy provides the capability to measure simultaneously the temperature and the concentrations of all major species with high temporal and spatial resolution in sub- and supersonic flames.

2.4. Investigation of the flame structure and the flame length

The flame length is another vital design criterion for sizing combustors. The length of the combuster should be long enough for the flames to react completely inside the chamber. The presence of superequili-

brium OH radicals indicats the structure and the length of sub- and supersonic flames. The investigation of OH radicals can also provide useful informations about finite-rate chemistry effects in the turbulent flames. Laser-induced fluorescence (LIF) is used for example to measure the OH concentration of highly turbulent flames with adequate temporal and spatial resolution (fig 5).

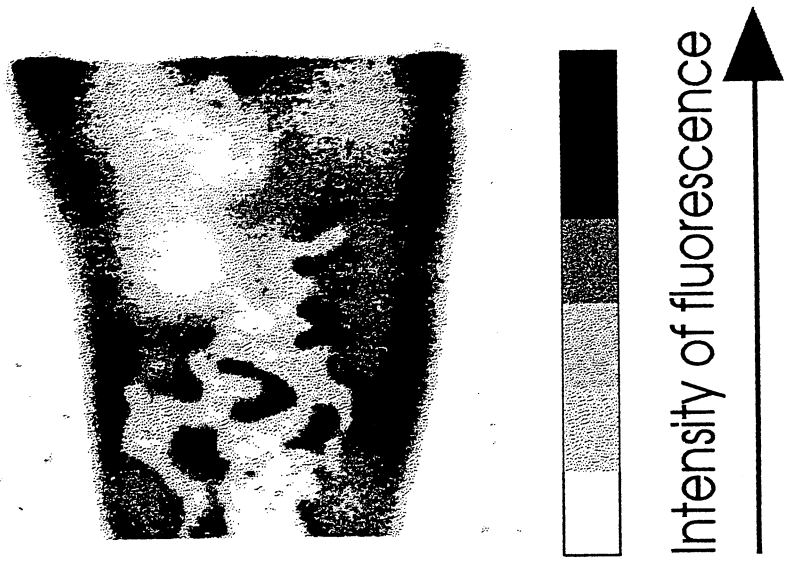

Fig 5: OH radicals in a diffusion flame

3. Overview of optical measurement techniques

To select the best suitable technique for a given problem, the first point of interest in a measurement problem is the determination of the characteristic parameters of the process to be investigated. Parameters may be the temperature distribution in the flame or the concentration of certain species in the reacting flow. Each of the following items should be answered before starting the selection of the most suitable technique:

- required accuracy of measurement
- required time resolution
- required spatial resolution
- overall dimensions of the measuring volume
- maximum duration of measurement
- optical accessability of measurement volume

Figure 6 shows a summary of optical techniques, as well as the physical process on which the technique is based. Furthermore the most common applications for each technique and the dimensions of the measurement and whether real-time application is possible are listed.

measuring technique	physical effect	application	dimension	real-time application
Shadowgraph	light deflection	heat, mass transfer	2d (integ.)	yes
Interferometry	refraction and change of vel.	heat, mass transfer	2d (integ.)	yes
Raman scattering	Raman scattering	concentration temperature	piont - 1d	no
Laser induced Fluorescence	Fluorescence	concentration temperature	piont - 2d	no
Self Fluorescence	therm. Fluores. chemolum.	concentration temperature	2d (integ.)	yes

Fig 6: Overview of optical methods

4. Raman diagnostic

Raman spectroscopy is mostly applied to molecules because of the characteristic behavior of molecules with regard to their possible energetic states. Common to all molecules are specific, discrete rotational and vibritional energy levels, which causes the frequency shift between the scattered and the incident light to be corresponding to the observed molecule. This feature of Raman scattering makes it possible to investigate different species simultaneous in a single measuring volume.

NOMENCLATURE

A	transition probability
B_e	rotational constant
$b_{J+\Delta J,J}$	Placzek coefficient
c	speed of light
C_n	proportionality constant of specific setup
D_e	rotational constant
$E(v,J)$	energy content of the term specified by the rotational and vibrational quantum numbers v and J
$g_i(J)$	statistical weight factor of the rotational term due to nuclear spin
h	Plancks constant
I_R	intensity of the registered Raman signal
I_0	intensity of the laser light
k	Boltzmann constant
l	length of the measuring volume
N	number density of molecules
$N_{v,J}$	number density of molecules in the energy state with the vibrational and rotational quantum numbers v and J
Q_J	rotation partition function
Q_v	vibration partition funktion
T	absolute temperature in thermodynamic equilibrium
T_{rot}	ratational temperature
T_{vib}	vibrational temperature
v	quantum number of the vibrational energy state
x_e	second order coefficient of the virational energy term
y_e	third order coefficient of the virational energy term
α	molecular polarizability tensor
α_e	coefficient for vibrationg rotor
β_e	coefficient for vibrationg rotor
γ_v	coefficient for the regarded vibrational transition
λ_0	wavelength of the icident (laser-)light
λ_R	wavelength of the raman signal
ν_0	frequency of the icident (laser-)light
$\tilde{\nu}_0$	wavenumber of the icident (laser-) light
$\Delta\tilde{\nu}_R$	Raman shift in wavenumbers
$\frac{d\sigma}{d\Omega}$	differential scattering cross section
Ω	solid angle of the collection optics
ω_e	vibrational constant

4.1. PRINCIPLES OF THE MEASUREMENT TECHNIQUE

An understanding of Rayleigh and Raman scattering is best, provided by a simplified model of energy exchange during the interaction of a molecule and light hitting the molecule. Each molecule exhibits discrete energy levels within the ground electronic state (higher electronic states are not regarded in

Raman scattering). The energy of a molecule is stored in part as rotational and in part as vibrational energy yielding a specification of the energy state by one rotational (J) and one vibrational quantum number (v). The energetic difference between adjacent rotational levels is much smaller than between adjacent energy levels, therefore each vibrational level contains many rotational levels. For a diatomic molecule the distribution of possible energy levels with their respective quantum numbers (v, J) are schematically shown in fig. 7. The energy content of a specific term $E(v, J)$, devided by $h \cdot c$ (h = Planck's constant; c = speed of light) and expressed in $[cm^{-1}]$, is Ledermann [1980]:

$$\begin{aligned} E(v,J) &= \omega_e(v+1/2) - \omega_e x_e(v+1/2)^2 + \omega_e y_e(v+1/2) + \cdots \\ &\quad +[B_e - \alpha_e(v+1/2)]J(J+1) - [D_e + \beta_e(v+1/2)]J^2(J+1)^2 \\ &\quad +2D_e/3\omega_e^2(12B_e^2 - \alpha_e\omega_e)J^3(J+1)^3 + \cdots \end{aligned} \tag{1}$$

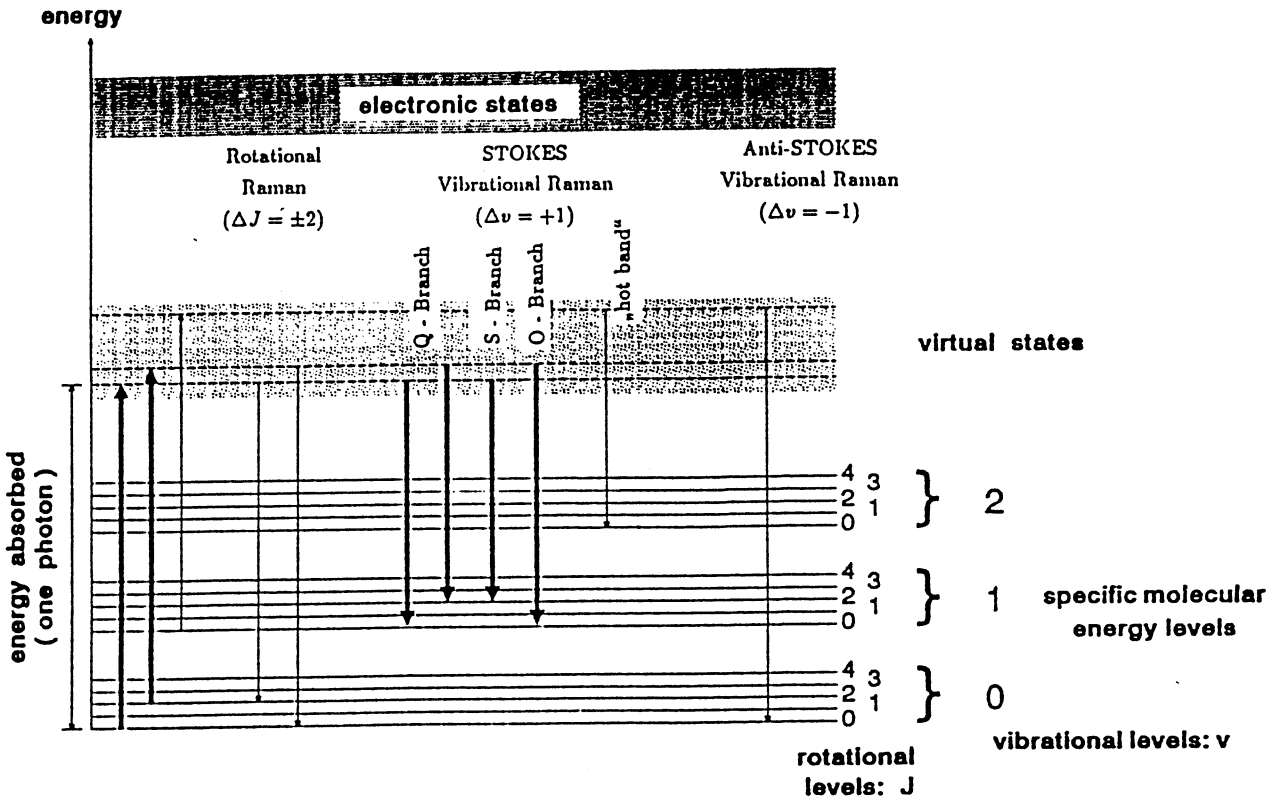

Fig 7: Simplified energy model for a diatomic molecule and possible transitions

Except for the quantum numbers v and J all quantities in equ. 1 are molecular constants. ω_e, B_e and D_e are characterized by mass of the involved atoms and their bond structure. $\omega_e x_e$ and $\omega_e y_e$ in the vibrational terms represent deviations from an ideal harmonic oscillator, α_e and $\beta_e$represent rotation-vibration coupling. A more detailed comprehensive discussion of the structure of molecules can be found for example in Alonso [1988] or Herzberg [1966]. However, in order to perform Raman scattering experiments a detailed knowledge of the involved quantum mechanics is not absolutely necessary; usually the values for the expected Raman shifts can be obtained from tables found in the literature Demtröder [1991].
Now the events occuring in the scattering process shall be discussed. In the beginnig the molecule is assumed to be in its energetic ground state and the incoming light to be monochromatic of wavelength λ_0 (or wave number $\tilde{\nu}_0(\tilde{\nu}_o = 1/\lambda_0)$). The molecule absorbs one photon of the incident radiation with an energy content of $E = h \cdot c \cdot \tilde{\nu}_0$. This energy absorption lifts the molecule to a virtual state above the stable states of the ground electronic state, but below the first electronic state. Within a very short period of time ($\sim 10^{-14}s$; Ledermann [1980]) the molecule returns from this virtual state to a stabel energetic

state within the ground electronic state, this time emitting one photon of light. If the original and the new energy state are identicall, the amount of energy emitted is equal to the amount of energy originally absorbed. Due to the proportionality of Energy and wave number this equality implies the wave number or wave length of the incident and emitted radiation are equal as well. If the final energy state of the molecule meaning the emitted photon contains less energy than the absorbed photon. This leads to wave number (or wavelength) shift $\Delta\tilde{\nu}_R(\Delta\lambda_R)$ of the emitted light compared to the incident light:

$$\Delta\tilde{\nu}_R = E(v,J) - E(v+\Delta v, J+\Delta J) \tag{2}$$

For wavelength at which the Raman signal appears λ_R, the following formula is applicaple Leipertz [1981]:

$$\lambda_R = (\frac{1}{\lambda_0} - 1.0003\Delta\tilde{\nu}_R)^{-1} \tag{3}$$

If the final molecular state is above the original state, the wave number shifts to lower values (higher wavelength; "red-shift"), if the molecule is originally in an elevated energetic state and returns to a lower state, the shift is toward higher wave numbers (lower wave-length; "blue-shift"). In spectroscopy a red-shift is called "Stokes"-transition, a blue-shift is called "anti-Stokes"-transition.
Quantum mechanical considerations only allow a number of molecular transitions. For a diatomic molecule these transitions are $\Delta\nu = 0, \pm 1$ and $\Delta J = 0, \pm 2$ and are included in the diagram fig. 7. A transition characterized by $\Delta\nu = 0$ and $\Delta J = 0$ represents Rayleigh scattering, transitions with $\Delta\tilde{\nu} = 0$ and $\Delta J = \pm 2$ are pure rotational Raman transitions (Stokes or anti-Stokes branch). Vibrational transitions are characterized by $\Delta\nu = \pm 1$, where pure vibrational transitions ($\Delta J = 0$) are called Q-branch and vibrations-rotation transitions with $\Delta J = +2$ or $\Delta J = -2$ are called S-branch or O-branch respectively.

Concentration Measurements Since the difference between the energy levels of a molecular species is characteristic for the molecule depending on the atoms and the acting forces in the molecule, the wave number shifts encountered in Raman scattering are also characteristic for the molecule considered. The vibrational Raman signals can usually easily be spectrally resolved due to the relatively large difference in wave number shift.
Fig. 8 shows the spectral position of the first Stokes vibrational Q-branch ($\nu = 0 \rightarrow \nu = 1; \Delta J = 0$) of technically important gases when an excimer-laser (XeCl) with a wavelength of 308 nm is used. Longer laser wavelengths lead to bigger spectral distances between the signals, at the same time, however, the intensity of the Raman signals decreases. If the Raman lines of two species are very close together (i.e. CO_2 and N_2O at 320.7 nm), usually there are other transitions suitable for spectroscopic purposes (CO_2 at 321.8 nm and N_2O at 330.7 nm).

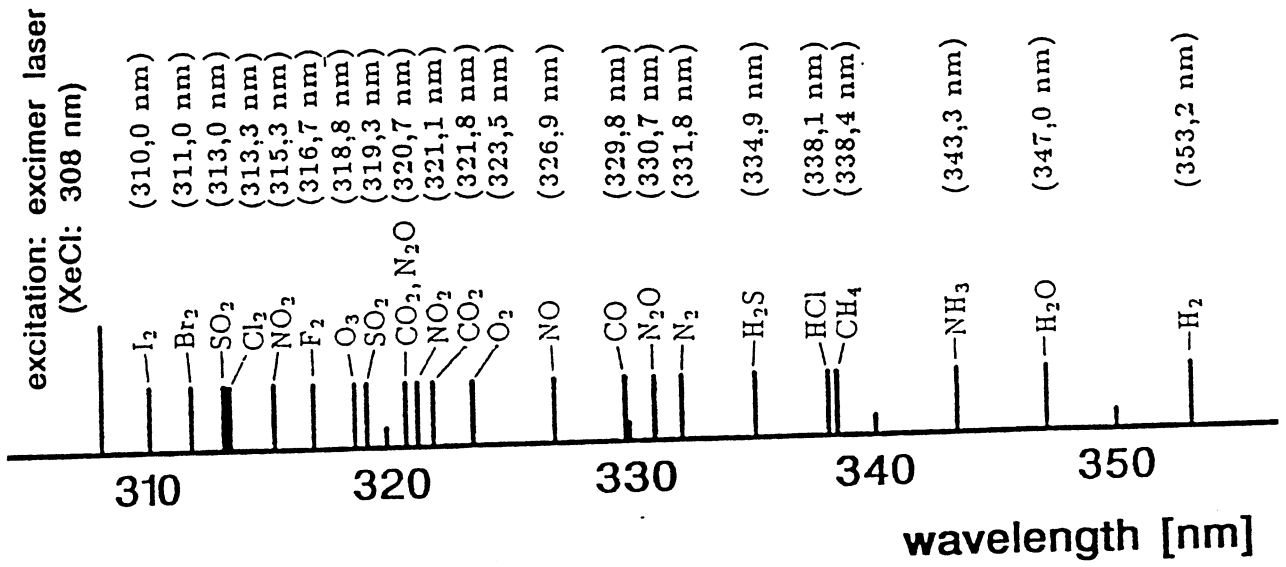

Fig 8: Wavelength of the Stokes Q-branch for technically important gases when excited with an excimer laser (XeCl) at 308nm.

The intensity I_R of the observed Raman signal is proportional to the differntial cross section $d\sigma/d\Omega$ of the molecule, the solid angle of observation Ω_E, the observed length of the measuring volume l, the number density of the molecules in the initial energy level $(\nu, J)N_v, J$, the irradiance of the laser beam I_0. The proportionality factor C_1 represents the efficienty of the detection system yielding the following equation:

$$I_R = C_1(\frac{d\sigma}{d\Omega}) \cdot l \cdot N_{v,J} \cdot I_0 \tag{4}$$

The differental cross section $d\sigma/d\Omega$ depends on the strength of the interaction between the incident radiation and the considered molecule in the energetic state before the transition. Beside yielding values for the calculation of the absolute signal intensity of a specific transition the differential cross section is important for the derivation of the formulae used to determine concentrations and temperatures from the obtained Raman spectra. Generally intensity ratios of two specific signals are used for these measurements; therefore the values of the proportionality factors used in equations 4 and 5 are not important as long as the same experimental setup is used for all the measurements. The differential cross section is:

$$\frac{d\sigma}{d\Omega} = C_2 \cdot \tilde{\nu}_R^4 \cdot \gamma_v \cdot A(b_{J+\Delta J,J}, \alpha) \tag{5}$$

$\tilde{\nu}_R$ is the wave number of the scattered radiation ($\tilde{\nu}_R = \tilde{\nu}_0 \pm \delta\tilde{\nu}_R$), γ_v is a factor for the regarded vibrational transition (Stokes: $\gamma_v = v + 1$; anti-Stokes: $\gamma_v = v$) and the factor A describes the transition probability depending on the regarded rotational transition and polarization considerations for the setup used. Here $b_J + \Delta J, J$ denotes Placzek coefficient, α the molecular polarizability tensor. A detailed discussion is given by Long [1977].

Generally intensity ratios of two specific signals are used for these measurements; therefore the values of the proportionality factors used in equations 4 and 5 are not important as long as the same experimental setup is used for all the measurements.

The number of molecules N_v, J in the regarded energy level (v, J) can be obtained from thermodynamical statistics according to the Boltzmann distribution function as

$$N_{v,J} = N \cdot g_i(J) \cdot (2J+1) \cdot \frac{\exp[-hcE(v,J)/kT]}{Q_v \cdot Q_J} \tag{6}$$

where N is the number density of molecules of the regarded species. The therms $g_i(J)$ and $(2J+1)$ result from degeneracies of the rational state J Long [1977]. Q_v and Q_J are the rotational and vibrational partition functions

$$Q_{v,J} = Q_v \cdot Q_J = \sum_v \sum_J g_i(J) \cdot (2J+1) \cdot \exp[-hcE(v,J)/kT] \tag{7}$$

with h as Planck's constant, c the speed of light, k Boltzmanns's constant, $E(v,J)$ the energy of the state with the quantum numbers v ,J and T as the absolute temperature. Equations 4 through 7 yield

$$I_R = C_3 \cdot \tilde{\nu}_R^4 \cdot \gamma_v \cdot A(b_{J+\Delta J,J}, \alpha) \cdot I_0 \cdot N \cdot \frac{g_i(J)(2J+1)\exp[-hcE(v,J)/kT]}{\sum_v \sum_J g_i(J) \cdot (2J+1) \cdot \exp[-hcE(v,J)/kT]} \tag{8}$$

Equation 8 shows that for a given experimental setup and constant temperature the intensity of a Raman line is directly proportional to the number of molecules in the measuring volume, i.e. species concentration. Therefore a detailed knowledge of all factors in the above equations is not necessary. It is sufficient to calibrate the setup at known temperature and pressure for each species expected in the investigated system. If lower accuracy of the measurements is sufficient for the purpose of the investigations, a simple calibration using nitrogen as a reference may be made. Then the Raman signals from the actual species have to be multiplied by calibration factors accounting for the differing Raman cross sections of nitrogen and the species.These factors have been measured for many species at various laser wavelength and are available from the literature Huber [1979].

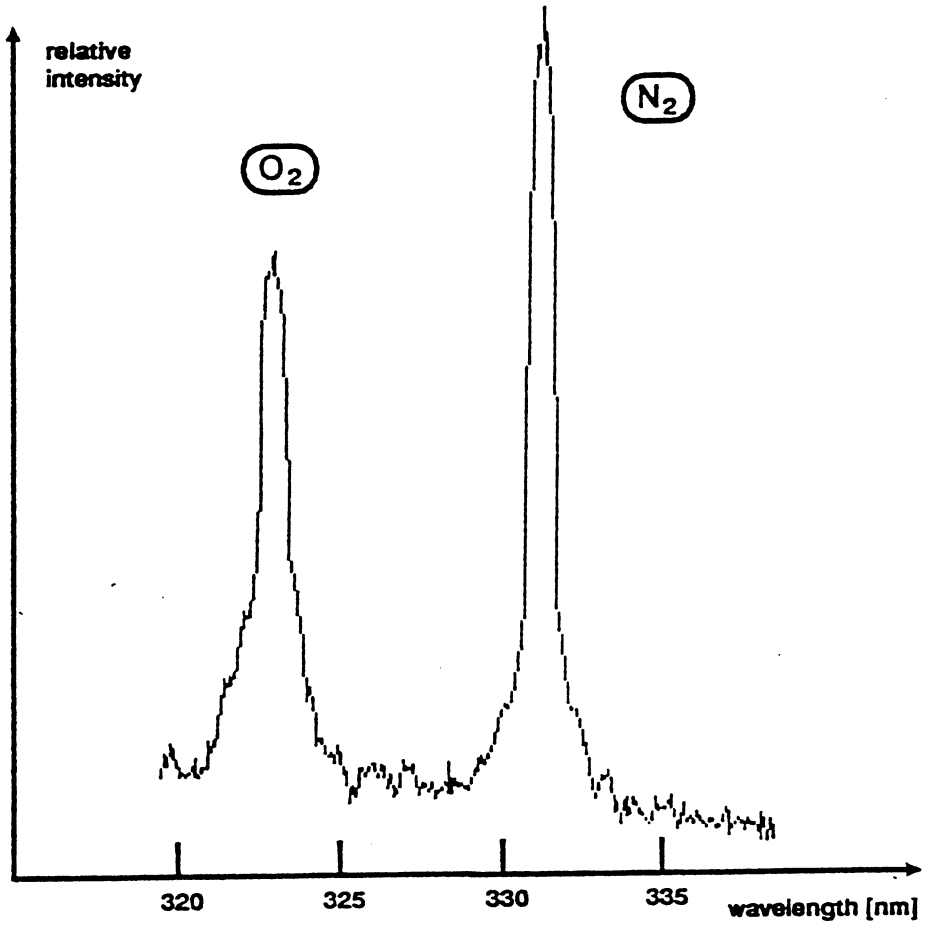

Fig 9: Stokes vibrational spectrum (unresolved rotational lines) of air at ambient temperature and pressure (raw data); $\lambda_0 = 308$ nm. The differential cross section for oxigen and nitrogen are approximately the same, if the peaks are corrected for the quantum efficiency of the detection systems and scaled according to the λ^4 relation.

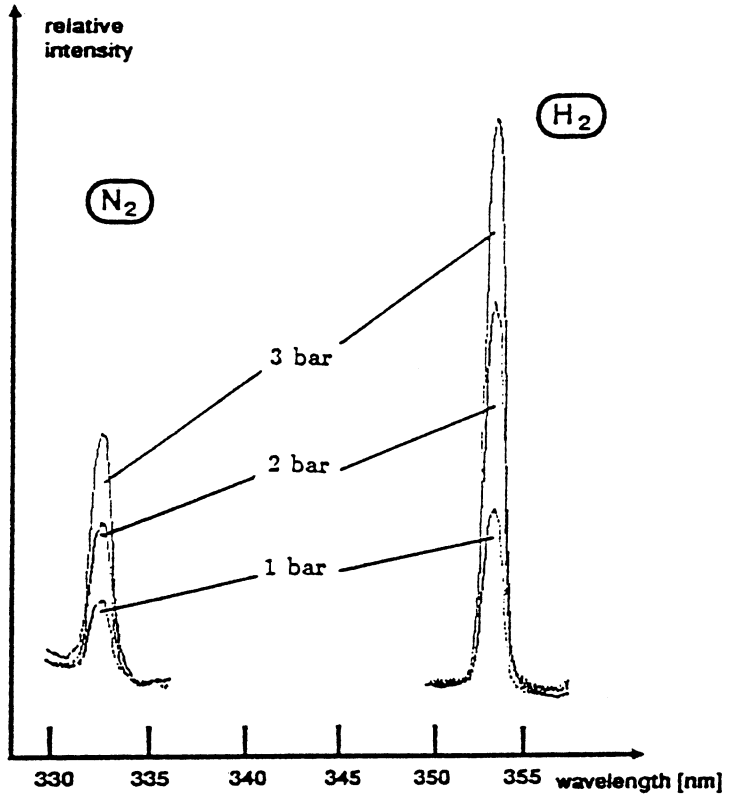

Fig 10: Stokes vibrational spectra of nitrogen hydrogen at ambient temperature and various initial pressures; $\lambda_0 = 308nm$. The linearity of the spontaneous Raman effect can be clearly seen: the intensity of the Raman signal (area underneath the peak) rises constantly with the pressure. Also, the differntial cross section of hydrogen is approximately four times higher than that of nitrogen.

Fig. 9 shows vibrational spectra of air at ambient conditions with the rotational lines unresolved. The ratio of the intensity of the oxygen and nitrogen Raman signals (marked area underneath peak) is equivalent to their concentration ratio in the gas after correction for the deviations in quantum efficiency of the detection system and scaling according to the δ^4 relation are made.This means the cross sections for oxygen and nitrogen are the same. This is not the case for nitrogen and hydrogen as can be seen in fig.10. This figure shows the Stokes vibrational Raman spectra of nitrogen and hydrogen at ambient temperature and pressures of 1, 2 and 3 bar. The differntial cross section of hydrogen is about four times higher than that of nitrogen. The spectra in fig. 10 also show the linearity of the Raman effect. Since the measuring volume and the temperature are held constant during the experiments, the number of molecules in this volume is proportional to the pressure and again proportional to the Raman signal. If the pressure of the investigated medium is constant, the vibrational Raman spectrum of a non reacting species yields temperature information due to the inverse proportionality between temperature and density provided by the equation of the ideal gas. However, at higher temperatures where a significant number of molecules may initially be upper state bands, the $(v + 1)$ factor in the transition intensity equations leads to errors if it is not accounted for.

Temperature Measurement The measurement of temperture with Raman scattering is possible due to the temperature dependence of the population distribution of the energy levels of the molecules. This population distribution is described by the Boltzmann equation and is included in equation 6. Fig. 11 shows the population of the vibrational energy levels at various temperatures, fig. 12 the population of the rotational levels for ocxygen, nitrogen and hydrogen. Equation 6 can be applied to evaluate the temperature of a system by comparing the intensities of different Raman trasition signals. If only vibrational transitions are used, the vibrational temperature is obtained, if rotational transitions are used the rotational temperature is obtained. For systems in thermodynamic equilibrium the rotational and the vibrational temperature are equal. Only in high-velocity flow field (supersonic nozzles etc.) or in highly reactive systems (combustion processes) the vibrational temperature with a relaxation time of $10^{-6}s$ may be 'frozen' while the rotational temperature with a relaxation time of $10^{-8}s$ is not Leipertz [1981]. The differential scattering cross-section of rotational transitions are at least one order of magnitude larger than those of vibrational transitions, yielding a much higher signal/noise ratio. Therefore thermometry by rotational Raman scattering usually gives more accurate results than thermometry by vibrational Raman scattering. On the other hand, the rotaional lines of the different species tend to interfere with each other, especially in systems with many different species. There is no general rule of preference to either of the methods.

Thermometry by Rotational Raman Spectroscopy If a pure rotational Stokesd transition within the ground vibrational state is regarded ($\Delta v = 0; \Delta J = 2$) the application of equations 1 and 8 gives the intensity of the Raman signal of the initial rotational level J as:

$$I_{R,S}(J) = C_4 \cdot (\tilde{\nu}_0 - \Delta\tilde{\nu}_R)^4 \cdot I_0 \cdot N \cdot \frac{(J+1)(J+2)}{(2J+3)} \cdot g_i(J) \cdot \frac{\exp[-hcBJ(J+1)/kT_{rot}]}{Q_J} \tag{9}$$

Here $B = B_e - 1/2\alpha_e$, the other terms of equation 1 involving the quantum number J are neglected. The term $(J+1)(J+2)/(2J+3)$ results from the Placzek coefficient for the transition $\Delta J = +2$ Long [1977] All factors in equation 8 which refer to vibrational transitions are included in the proportionalty constant C_4.

The rotational temperature is obtained by comparison of the intensity of transitions from two differnt initial energy levels $E(v, J_1)$ and $E(v, J_2)$. Since the measurement of both transitions are done under the exact same conditions the factors C_4, I_0, N, Q_J of equation 9 are identical for both transitions and therefore cancel each other:

$$\frac{I_{R,S}(J_1)}{I_{R,S}(J_2)} = \frac{(\tilde{\nu}_0 - \Delta\tilde{\nu}_R(J_1))^4 \cdot \frac{(J_1+1)(J_1+2)}{(2J_1+3)} \cdot g_i(J_1) \cdot exp[-hcBJ_1(J_1+1)/kT_{rot}]}{(\tilde{\nu}_0 - \Delta\tilde{\nu}_R(J_2))^4 \cdot \frac{(J_2+1)(J_2+2)}{(2J_2+3)} \cdot g_i(J_2) \cdot exp[-hcBJ_2(J_2+1)/kT_{rot}]} \tag{10}$$

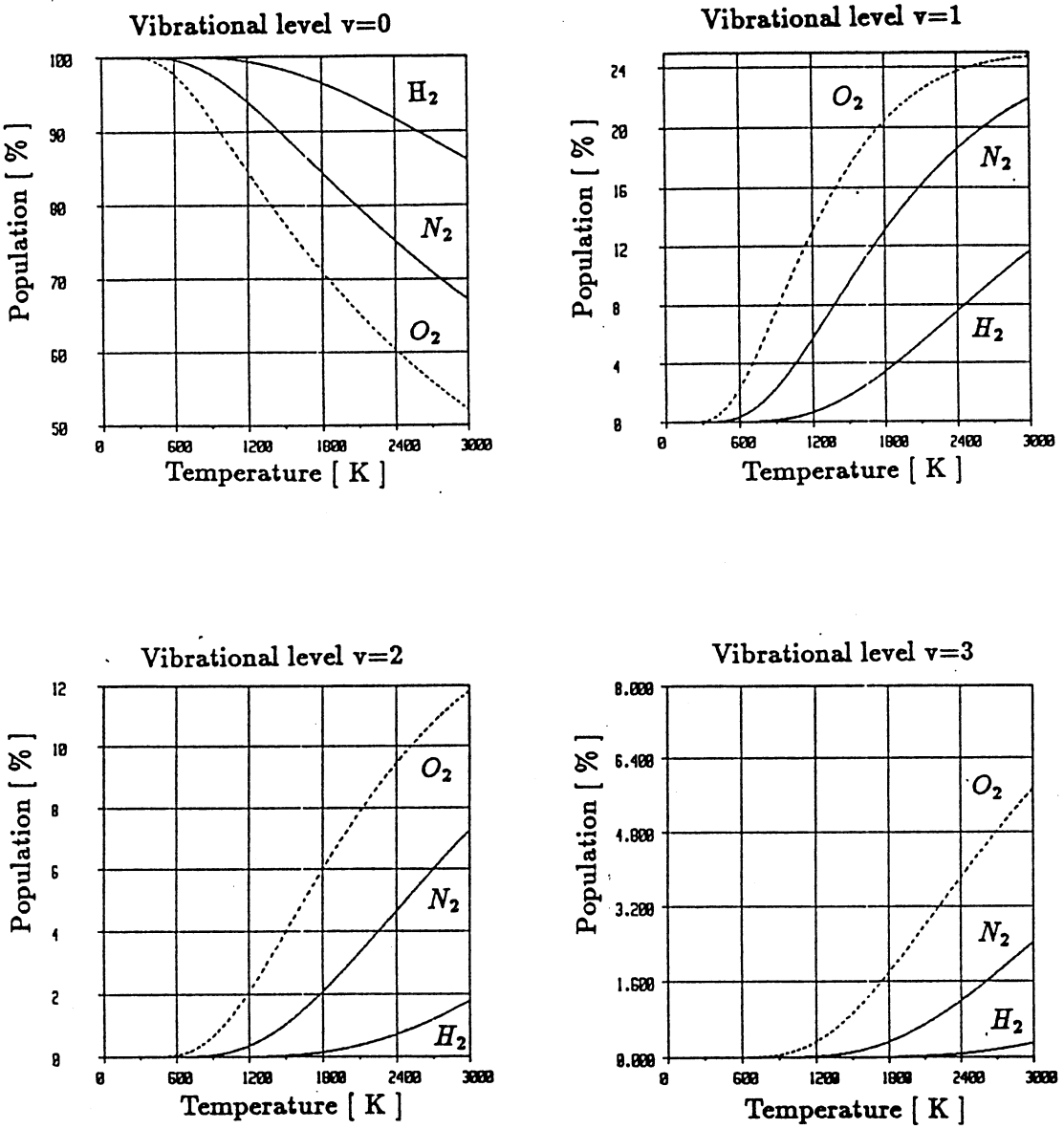

Fig 11: Population distribution of vibrational energy levels (v) as a function of temperature for O_2, N_2 and H_2

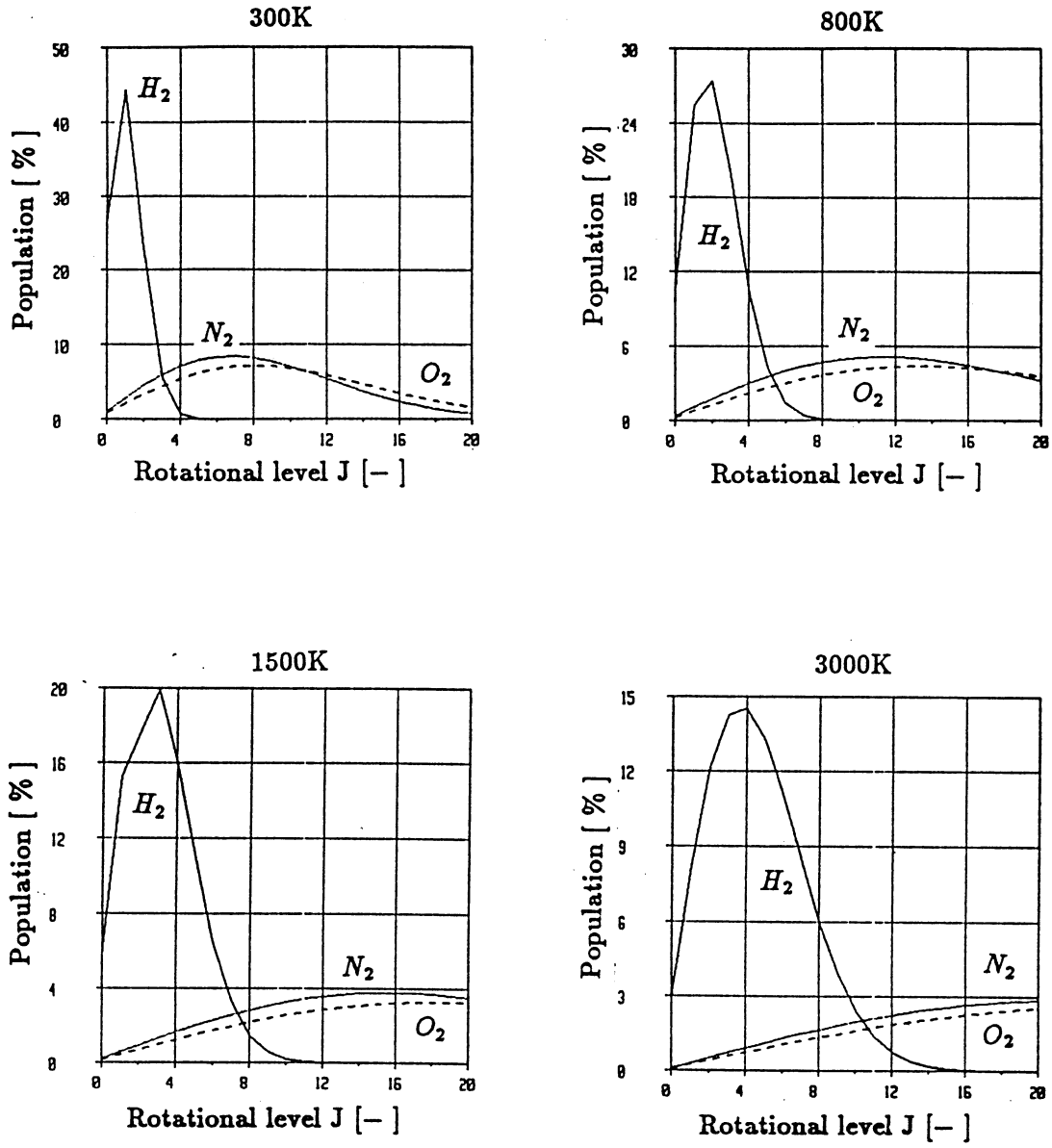

Fig 12: Population distribution of the rotational levels (J) at T = 300, 700, 1000 and 3000 K for O_2, N_2 and H_2

The resulting Raman shift $\Delta\tilde{\nu}_R$ from a rotational transition with $\Delta J = +2$ is $\Delta\tilde{\nu}_R = 4B(J + \frac{3}{2})$. If equation 10 is solved for the temperature T_{rot} this becomes:

$$T_{rot} = [(J_2)(J_2+1) - (J_1)(J_1+1)] \cdot \frac{h \cdot c \cdot B}{k} \cdot \left\{ ln[\frac{I_{R,S}(J_1)}{I_{R,S}(J_2)} \cdot \left(\frac{g_i(J_2)}{g_i(J_1)} \cdot \frac{(2J_1+3)(J_2+1)(J_2+2)}{(2J_2+3)(J_1+1)(J_1+2)}\right) \cdot \left(\frac{\tilde{\nu}_0 - 4B(J_1+\frac{3}{2})}{\tilde{\nu}_0 - 4B(J_2+\frac{3}{2})}\right)^4] \right\}^{-1} \quad (11)$$

The temperature measurement becomes more reliable if it is done for several transitions and averaged. In analogy of the equations for the Stokes transitions for the anti-Stokes transitions can be obtained and measurements of the anti-Stokes band intensities can be utilized for thermometrie. Equation 10 can be

rewritten in the form:

$$J(J+1)\cdot\frac{1}{T_{rot}}=\frac{k}{hcB}\cdot\left\{-\ln[\frac{I_{R,S}(J)\cdot(2J+3)}{C_4\cdot g_i(J)\cdot(J+1)(J+2)[\tilde{\nu}_0-4B(J+\frac{3}{2})]^4}]\right\} \tag{12}$$

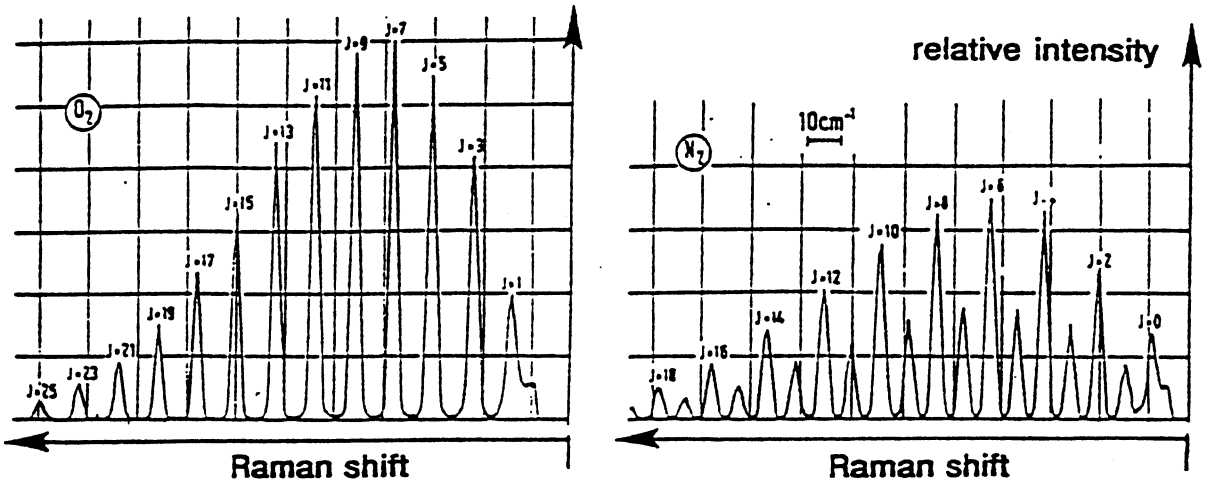

Fig 13: Stokes rotational Raman spectra of O_2 and N_2 at ambient temperature. J is the quantum number of the initial state. Here the influence of the nuclear spin, given by the term $g_i(J)$ in the equations, can be seen: N_2: $g_i = 6$ for even values of J, $g_i = 3$ for odd values of J; O_2: $g_i = 0$ for even values of J, $g_i = 1$ for odd values of J. Leipertz [1981]

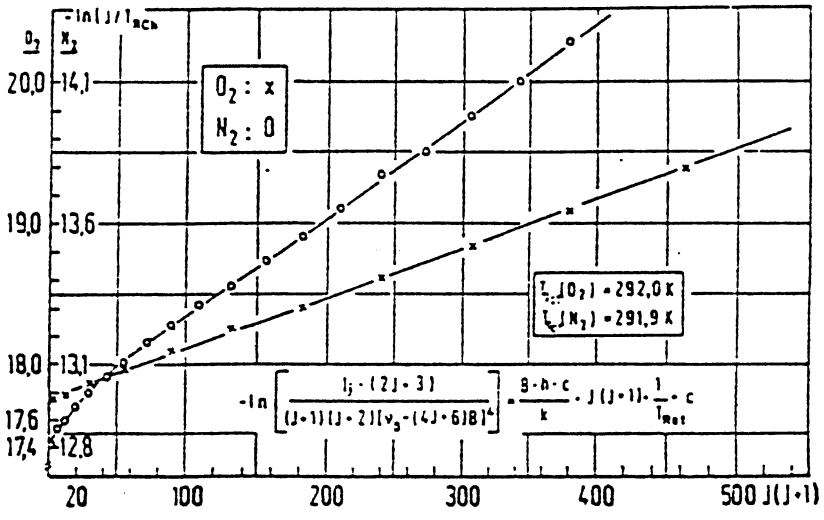

Fig 14: Determination of rotational temperature from spectra of Figure 13 Leipertz [1981]

If for every measured transition the right side of equation 12 is plotted against $[J(J+1)]$ the obtained points should lie on a straight line. The slope of this line is inversely proportional to the rotational temperature. Fig. 13 shows Stokes rotational Raman spectra of oxygen and nitrogen at ambient temperature (292 K) where especially the influence of the nuclear spin $g_i(J)$ can be clearly see. Fig. 13 shows the corresponding plot according to equation 12.

Thermometry by Vibrational Raman Spectroscopy The intensities of the Raman signals of the Stokes Q-branch ($\Delta v = +1, \Delta J = 0$) are given by (see equations 1 and 8):

$$I_R(v,J) = C_4(\tilde{\nu}_0 - \Delta\tilde{\nu}_R)^4 \cdot I_0 \cdot (v+1) \cdot \frac{J(J+1)}{(2J-1)(2J+3)} \cdot g_i(J) \cdot (2J+1) \cdot \frac{N \cdot \exp[-hc(\omega_e(v+\frac{1}{2}) + B\ J(J+1))/kT]}{Q_{vib} \cdot Q_{rot}} \tag{13}$$

Again the term energy has been introduced into the exponent in simplified form, consisting of a vibrational and a rotational term. Since the intensity of the Q-branch signals is about two orders of magnitude larger than that of the O- and S-branches, the Q-branch signals determine the shape of the recorded spectrum Laurendeau [1988] Due to the anharmonicities of the molecular vibrations the Raman shift of pure vibrational transitions decreases with increasing initial vibrational quantum number. In addition the (unresolved) rotational structure leads to a continous spectrum as it is schematically shown in fig. 15.

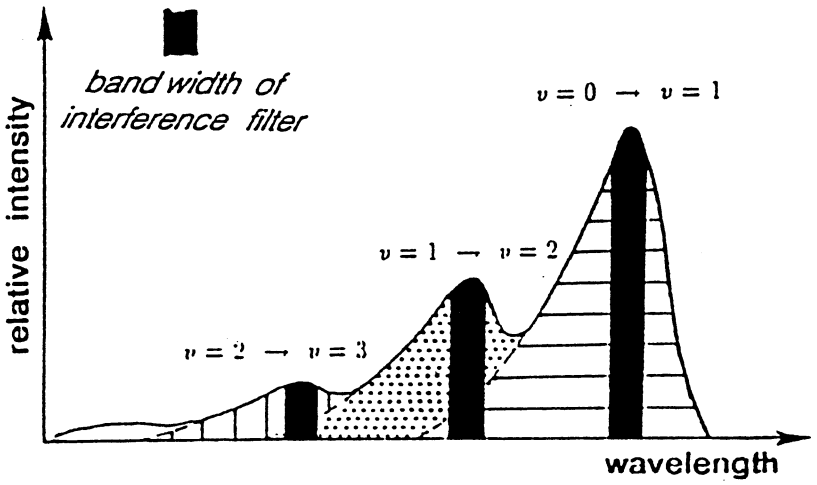

Fig 15: Schematic of a typical vibrational Q-branch spectrum as it appears at higher temperatures. The shaded areas indicate the obtained intensity when observation of the according bandwidth is made.

As with the rotational thermometry the vibrational thermometry is based on the temperature distribution of the molecules among the different vibrational states according to Boltzmann statistics. There are three basic vibrational thermometry methods: the contour fit method, the band-peak method of the 'hot-bands' and the Stokes/anti-Stokes method.

Using the contour fit method means to calculate the spectrum of the regarded molecule for various temperatures and fit it to the measured data as close as possible. In the calculations all parameters influencing the measurements have to be taken into account. Beside the actual scattering process these parameters include specific parameters of the experimental setup used such as the width of the registerd band pass of the quantum efficiency of the reception unit. Fig. 16 shows an example of a computer fit for the molecule of hydrogen obtained in flames. Due to the large constants for hydrogen, only the vibrational band from the ground state is observed. However, within this band the rotational lines can be resolved and compared to the theoretical curves.

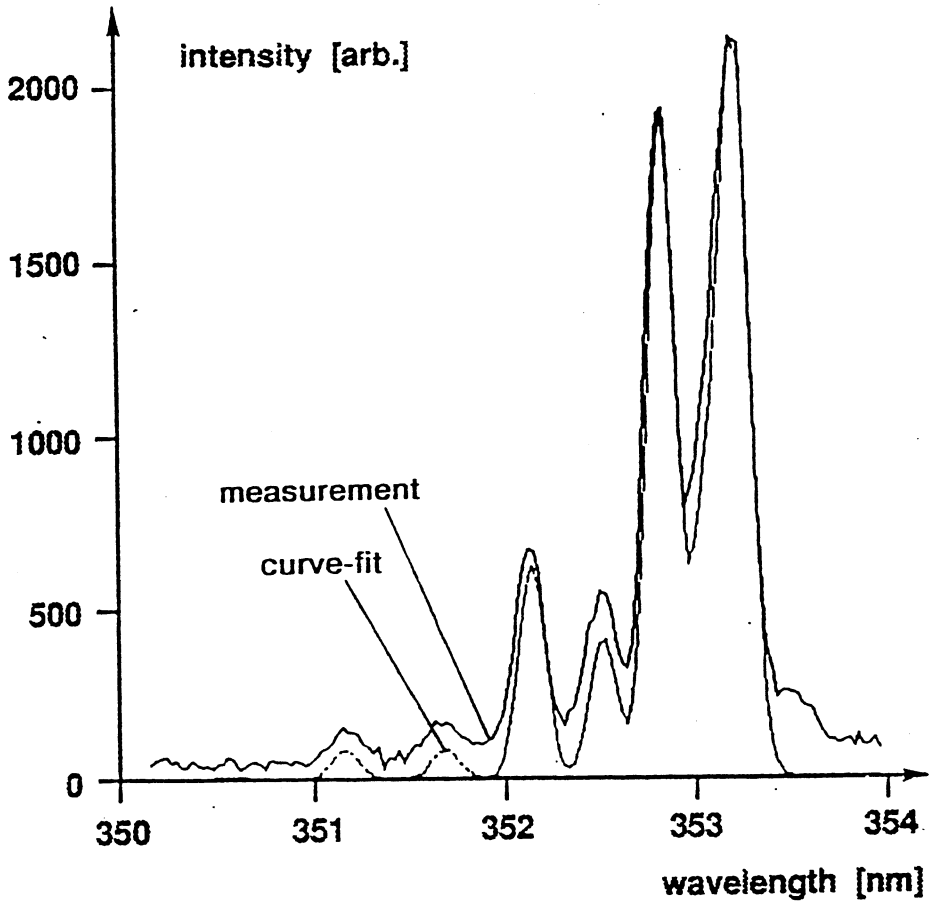

Fig 16: Stokes rotational-vibrational Raman spectrum of H_2 in a lean H_2-air flame. Due to the large rotational and vibrational constants of hydrogen only the vibrational transition from the ground level is observed; however, the rotational transitions within the vibrational band can easily be resolved. The temperature obtained from the theoretical curve fit was 960 K.

In applying the band-peak method the ratio of the Stokes Q-branch signals of differnt intial vibrational states is used to obtain the temperature of a system. For the signal intensities of all transitions from two adjacent vibrational energy levels equation 13 leads to:

$$\frac{I_R(v)}{I_R(v+1)} = \frac{(\tilde{\nu}_0 - \Delta\tilde{\nu}_{R,v})^4}{(\tilde{\nu}_0 - \Delta\tilde{\nu}_{R,v+1})^4} \cdot \frac{(v+1)}{(v+2)} \cdot \exp[\frac{-hc}{kT} \cdot \omega_e[v-(v+1)]] \tag{14}$$

The expression $\omega_e[v-(v+1)]$ is the same for all vibrational transitions from adjacent initial vibrational energy levels and equals the value for the vibrational Stokes Q-branch $\Delta\tilde{\nu}_R$ of the regarded species. The

expression $(\tilde{v}_0 - \Delta\tilde{v}_R, v)^4/(\tilde{v}_0 - \Delta\tilde{v}_R, v+1)^4$ is close enough to unity to be neglected. With the intensity measurement of two neighboring Q-branch transitions the temperature can be obtained from equation 16:

$$T = \frac{h \cdot c \cdot \tilde{\nu}_R}{k} \cdot \left(\ln \frac{I_R(v)}{I_R(v+1)} + \ln \frac{v+2}{v+1} \right)^{-1} \tag{15}$$

The above equation holds true for transition from any two adjacent vibrational energy levels, however due to the low population of higher energy levels measurements are generally limited to transitions from the ground and first, for some molecules also the second upper level. As can be seen in fig. 15 the intensity measured at the peak of the upper band includes some scattered light from the transition from the ground level. This has to be considered before using equation 16. An example for the temperature as a function of the Intensities of the Stokes Q-branch signals for nitrogen is given in fig. 17.

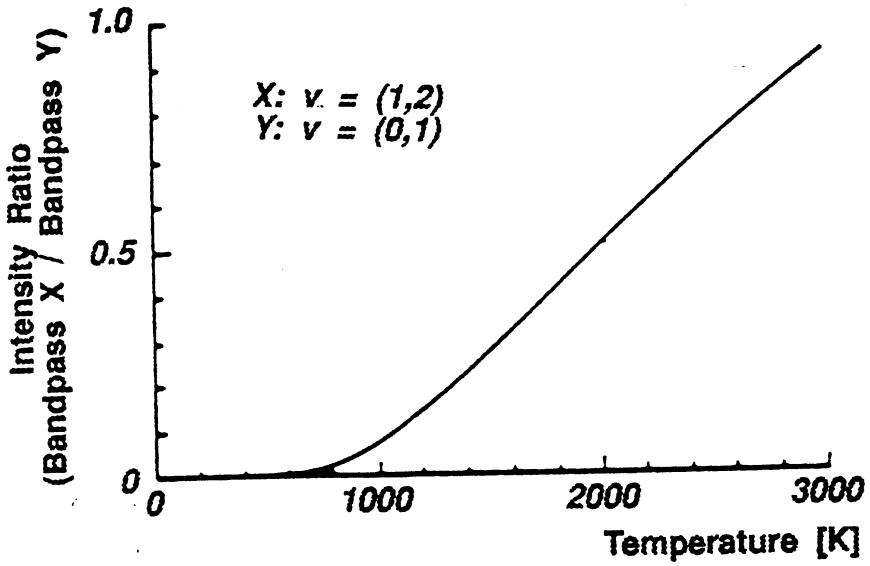

Fig 17: Calculated temperature as a function of the intensity ratio of the transitions from the ground and first upper vibrational level for N_2. The bandpass (0.2 nm) of the collected signal was centered at the wavelength of the intensity peaks (see fig. 15).

A third method of vibrational thermometry is possible when the ratio of the intensities from the vibrational Stokes bands and the vibrational anti-Stokes bands is taken to determine the temperature. For a conjugate pair of Stokes or anti-Stokes transitions (i.e. $V = 0 \rightarrow v = 1$ and $v = 1 \rightarrow v = 0$) the Raman shift $\Delta\tilde{v}_R$ is identical and the intensity ratio is in analogy to equation 15:

$$\frac{I_{R,S}(v)}{I_{R,aS}(v+1)} = C_5 \cdot \frac{(\tilde{\nu}_0 - \Delta\tilde{\nu}_R)^4}{(\tilde{\nu}_0 + \Delta\tilde{\nu}_R)^4} \cdot \exp[\frac{hc}{kT_{vib}} \cdot \Delta\tilde{\nu}_R] \tag{16}$$

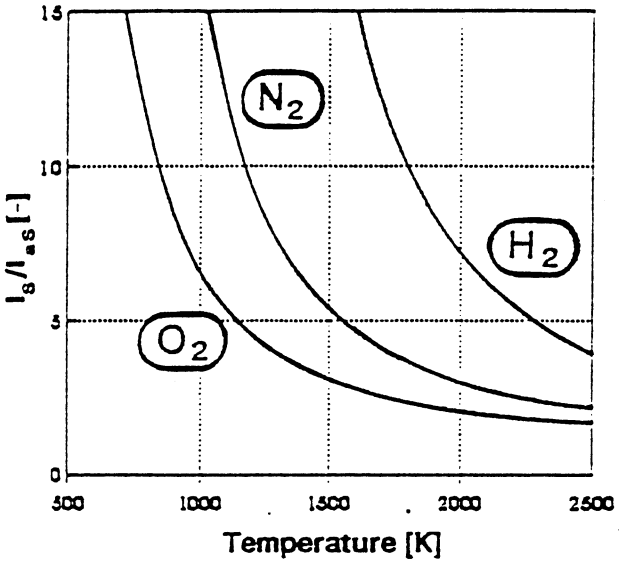

Fig 18: Calculated ratio of the intensities of the Stokes and anti-Stokes transitions as a function of temperature for H_2, O_2, N_2. The used excitation wavelength is that of an excimer laser (XeCl) at $\lambda = 308nm$. For other light sources the curves are shifted to other values due to the $\tilde{\nu}_0$ influence in equation 16.

The factor C_5 is introduced to take into account any differences in detection efficiency at the two wavelengths, since they are considerably far apart. For the temperature equation 17 yields:

$$T = \frac{h \cdot c \cdot \Delta\tilde{\nu}_R}{k} \cdot (\ln \frac{I_{R,S}}{C_5 \cdot I_{R,aS}} + 4 \ln \frac{\tilde{\nu}_0 + \Delta\tilde{\nu}_R}{\tilde{\nu}_0 - \Delta\tilde{\nu}_R}) \tag{17}$$

Since the intensity ratio is constant for all pairs of transitions, this method is also applicable without too much error when the vibrational band are not resolved. Therefore this method is suitable for all experimental conditions where a low signal intensity is expected, since the accumulated intensities of all transitions yield a higher level. Fig. 18 shows the calculated intensity ratios as a function of temperature for some diatomic molecules, the resulting curves for other molecules are similar to the ones shown.

4.2. Setup and examples of applications

Figure 19 shows a possible setup for spot (quasi-zero-dimensional) measurements of temperature and species concentration with Raman spectroscopy. The laser beam is focussed to a small spot, the diameter of which forms the cross section of the measuring volume, and is subsequently absorbed in a beam trap. The signal collection is usually arranged at a 90 ° angle to the direction of the laser beam. At this direction the signal intensity reaches a maximum and the size of the volume observed can be best determined. Even though for some specific applications the setup of two separate signal collection units may be useful, generally only one unit is necessary to conduct the measurements. If the specific construction containing the medium to be investigated allows the installation of a convex mirror opposite to the signal collection lens, the obtained signal intensity can be increased. In order to analyze the scattered intensities the collected light has to be resolved spectrally . This is accomplished either by diffraction units (i.e. polychromators) or selective filters. The intensity of the light at the selected wavelength then is converted into electronic signals, digitized and then numerically processed. For the necessary data acquisition and control routines

complete systems are commercially available.

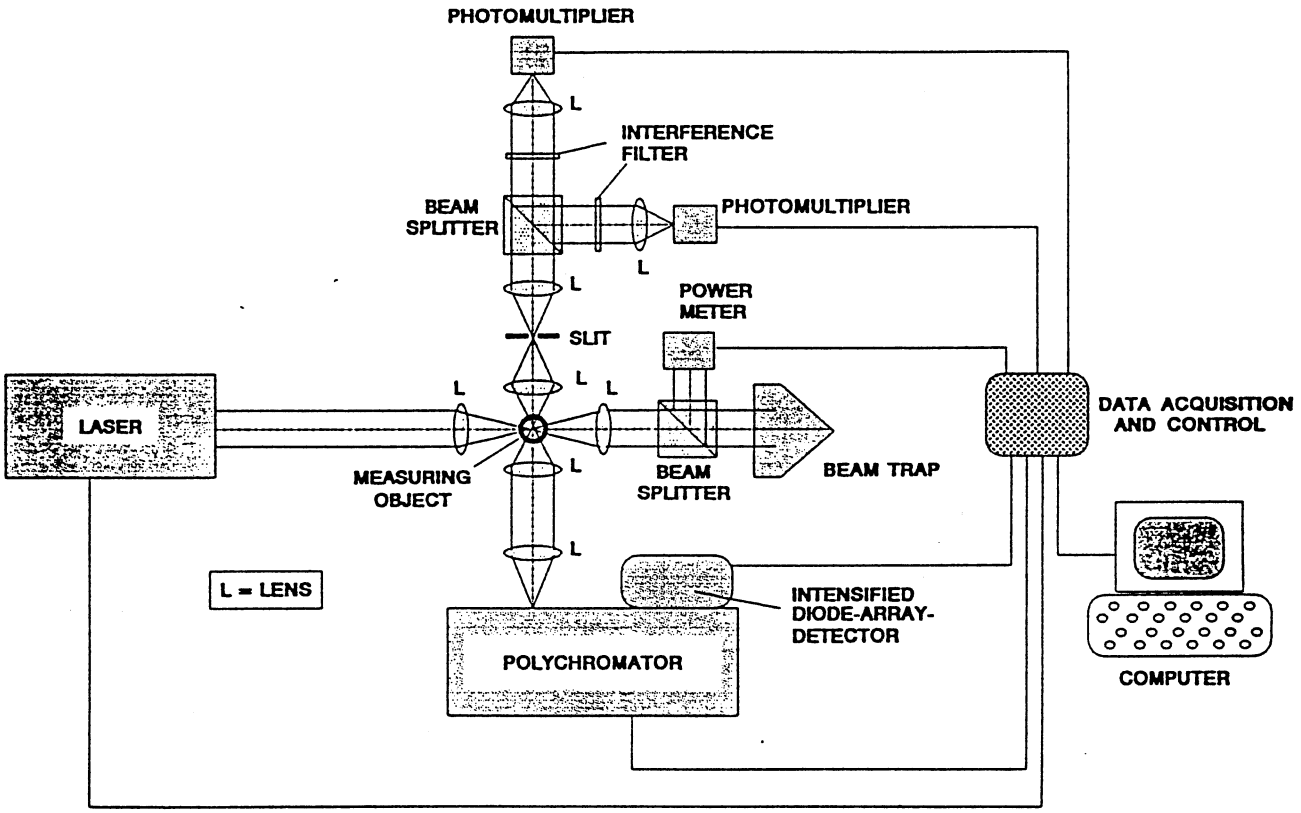

Fig 19: Typical Raman setup for point measurements. The two detection systems are only shown to demonstrate the different possibilities of arrangements, usually only one of the shown possibilities is used.

Raman spectroscopy is applied in a very wide variety of fields ranging from biology and chemistry for structural studies of molecules or reaction kinetic data, to engineering applications in determining the concentration and temperature distribution in flow fields containing several species simultaneously. Although the signal intensities decrease strongly with decreasing species concentration, i.e. increasing temperatures, the application of Raman scattering to reacting processes is one of the most important applications since measurements with conventional techniques often yield inadequate results.

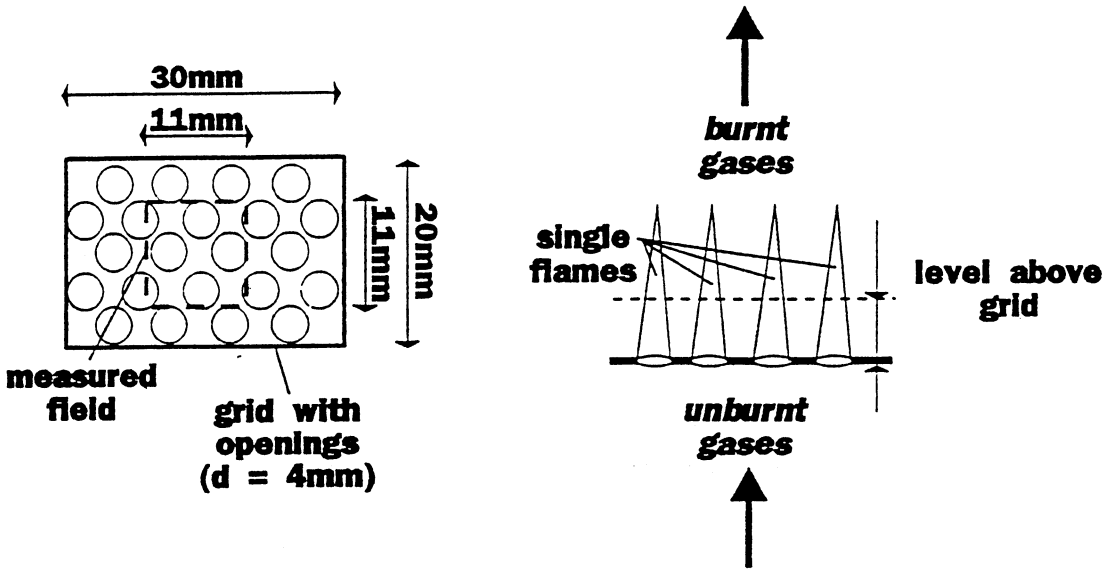

Fig 20: Arrangement of stationary operated burner with metal grids as flame stabilizing devices. Behind each opening a separate turbulent flame is formed. The flames are similar. Raman measurements have been taken in a three-dimensional array of location, the results of concentrations for each species is plotted for horizontal levels above the grid.

The next figures refer to combustion of H_2 in air. The experimental setup was a stationary operated, closed tube type burner with a rectangular cross section of 20 by 30 mm. A metal grid was used to stabilize the flame. Figure 20 shows the dimensions of the grid and the conditions around the grid. The premixed, unburnt gases with a hydrogen concentration of 12 Vol.% H_2 approach the grid upward with a velocity of 17 m/s. There is a separate turbulent flame stabilized behind each opening and the burnt gases leave the flame area upward. Raman point measurements have been taken in a three-dimensional array. The cross section of the array is represented by the dashed line in Figure 22, in which measurements have been taken at distances of 1 mm. The concentration distributions are depicted for each species in the form of levels with various distances from the grid (Strube [1989]).

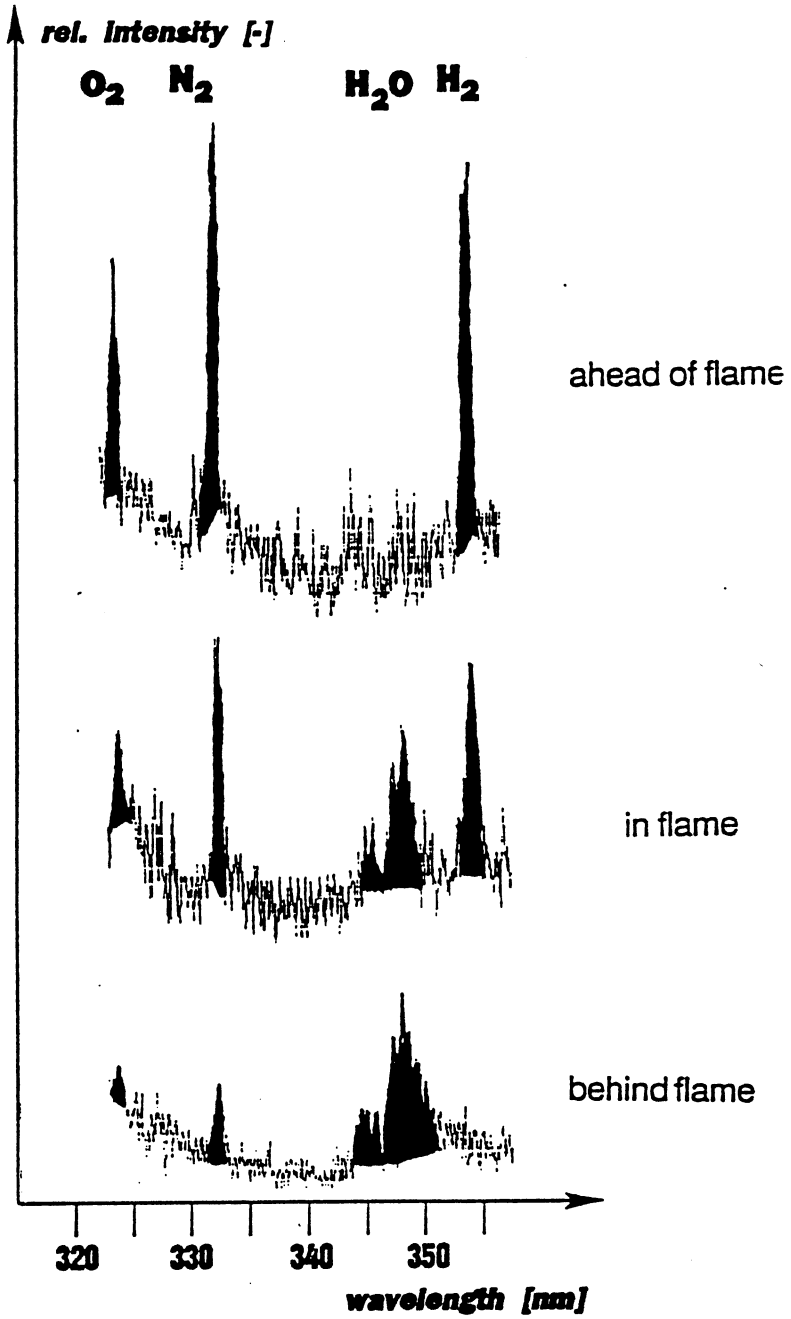

Fig 21: Typical spectra from representative points in the burner. Top: unburnt mixture with 12 Vol.% H_2 in air. Middle: spectrum from the turbulent reaction zone; the hydrogen has partially reacted with oxygen to form steam, so all species are present. Bottom: completely burnt mixture. The under-stoichiometric combustion leaves surplus oxygen, but there is no hydrogen left.

Figure 21 shows typical spectra of the characteristic zones. The first spectrum is taken before the grid; no combustion has taken place so there is no steam present. The second spectrum is taken from the reaction zone. Some of the hydrogen has reacted with parts of the oxygen to form steam as a product. All four species can be seen in the spectrum. The last spectrum is from a location above the reaction zone, the under-stoichiometric combustion is complete. Only steam, nitrogen and the surplus oxygen as species remain present. Assuming the nitrogen is inert, its concentration yields the temperature.

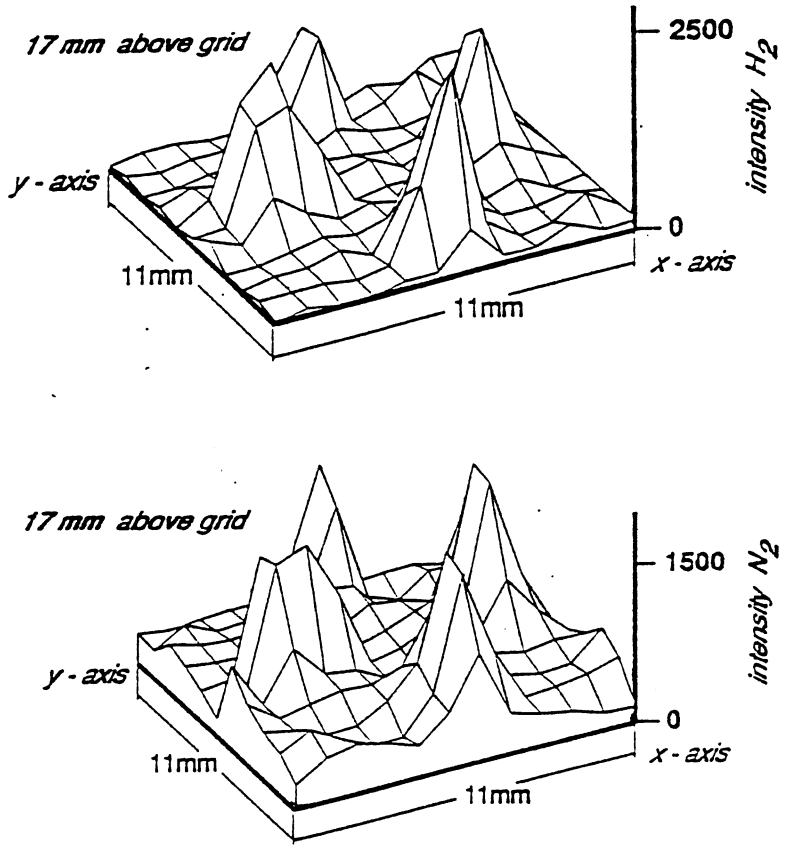

Fig 22: Nitrogen and hydrogen intensity distributions (equivalent to concentrations) obtained from measurements in a level 17 mm above the grid. The structure of the single flames is clearly visible. The nitrogen concentration is inversely proportional to the system temperature. It can be seen that the nitrogen spikes are broader than the hydrogen spikes, showing that the reaction mainly takes place at the surface of the conical flames.

Figure 22 shows, as an example, the nitrogen and hydrogen intensity distributions obtained from measurements in a level 17 mm above the grid. The integrated intensity from the spectra is proportional to the concentation of the regarded species. The structure of the single flames is clearly visible. In order to show the change in relative hydrogen concentration due to the combustion, the measured concentration of hydrogen has to be divided by the values for nitrogen. In the pictures it can be seen that the spikes of nitrogen are larger in diameter than those of hydrogen, indicating that the combustion mainly takes place at the conical surface of the single flames.

5. Self Fluorescence

The evaluation of the natural spontaneous emission of photons from particles in gaseous systems is one of the oldest optical measurement techniques for the determination of concentrations and temperatures. In 1857 Swan investigated the light emission of hydro-carbon flames and found distinct structures in the spectrally resolved emissions. The observed emissions in the visible range which are between 430 and 620 nm originated from C_2 molecules, as was found later. In any case these observations formed the basis for further investigations, mainly in high-temperature reacting environments.

In gaseous systems there is always a number of molecules or atoms in excited energy states. Some of these excited particles radiate energy by spontaneous emission of photons in connection with a change in the energetic state of the molecule. The emitted energy is always equal to the difference of the two energetic states involved. The wavelength of the emitted photon corresponding to a specific molecular transition can be obtained by Planck's equation to

$$\lambda = \frac{c \cdot h}{E_t} \tag{18}$$

If the light emitted from a specific spot of a system under investigation is spectrally resolved, conclusions can be drawn regarding the species, their concentration and temperatures. In self fluorescence the excitation of the molecules to the excited state may result from a number of different processes: thermal excitation (collisional process), absorption of light, chemical reaction (chemoluminescence) or dissociation/recombination. Since all of these processes occur simultaneously, in some cases the emission spectra have to be considered very carefully to obtain correct information on concentration and temperature. In this aspect self fluorescence is inferior to the newer laser techniques, since the latter employ only one specific excitation mechanism.

The major field of applications is the investigation of combustion processes as they appear in internal combustion engines, flight propulsion systems, power plants etc. The species observed are usually intermediate combustion products appearing only in the reaction zone and in very low quantities. The prime example of such a species is the OH radical which appears in virtually every technical combustion process.

Due to the rapid developmental advances in the fields of microelectronics and lasers, experimental investigations employing self fluorescence have been outperformed by laser scattering techniques very strongly. In comparison with these laser techniques self fluorscence is handicapped by several disadvantages, mainly the low spectral signal intensities leading to limited time and spatial resolution. However, if advanced detector technology is employed, very simple and versatile setups for self fluorescence spectroscopy can be used to obtain valuable information about the main processes even in very complex systems. The examples shown in this section are taken from different experiments involving hydrogen combustion with air. They exhibit the versatility of the measuring system used due to the application to both stationary and unstationary, sub- and supersonic as well as one and two-phase combustion.

NOMENCLATURE

A	first Einstein coefficient
B	second Einstein
B	rotational constant
c	speed of light
E	energy
FR	fluorescence rate
g	statistical weight factor
h	Plancks constant
I	intensity
J	rotational quantum number
k	Boltzmann constant
N	number density of molecules
P	rate of predissociation
Q	partition function
Q	rate of quenching transitions
T	absolute temperature in thermodynamic equilibrium
T	term energy
t	time
V	observed volume
v	quantum number
γ	mole fraction
λ	wavelength
η	efficiency
ν	frequency of light
$\Delta\tilde{\nu}$	laser band width
σ	collosional cross section
Ω	solid angle of collecting optics
ω_e	vibrational constant
e	electronic term
i	counting variable
J	rotational Energy level

SUBSCRIPTS

j	counting variable
L	Loschmidt
lin	linear LIF
pre	predissiciation LIF
S	regarded species
v	vibrational energy level

rot rotational states
sat saturated LIF
tot refering to all species
vib vibrational states
ν spectral function
0 laser light
1 lower energy state
2 upper energy state

5.1. Basic Principles of Self Fluorescence

Depending on the scatterer there are three types of natural spectra:

- line spectra
- band spectra
- continuous spectra

Line spectra result from electronic transitions in free atoms. The transitions are discrete resulting in distinct, sharp lines in the spectrum. Figure 23 shows schematically the visible part of the natural emission spectrum of atomic hydrogen. The lines correspond to transitions from higher states to the first excited electronic state and are called the 'Balmer'-series. The thickness of the lines shown represents qualitatively the intensity with which the lines appear, not the actual bandwith. Transitions from upper states to the ground state, the 'Lyman'-series, would show stronger intensity, appearing in the UV region between 97 and 122 nm.

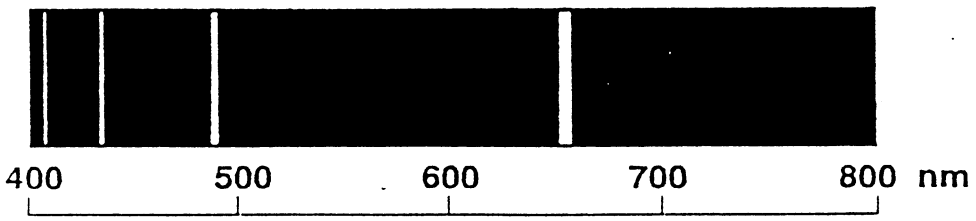

Fig 23: Visible emission spectrum of atomic hydrogen ('Balmer'-series); the thickness of the lines corresponds to the intensity of the lines, not their bandwith.

Since the energetic state of molecules, unlike atoms, can not simply be characterized by the electronic state, but also contain energy of vibration and rotation, the emission spectra of molecules consist of so-called bands instead of single lines. A typical band spectrum (of CH and C_2) is shown in Figure 24. If looked at with low spectral resolution, the bands seem to be continuous within their range. An increase in resolution, however, again exhibits a fine line structure within the bands. This is due to the discrete energy change also inherent to rotational-vibrational transitions during emission. Pure rotational-vibrational transitions, without a change of the electronic state, also yield band spectra; these bands appear in the infrared range, since the energy difference of the states involved is very small.

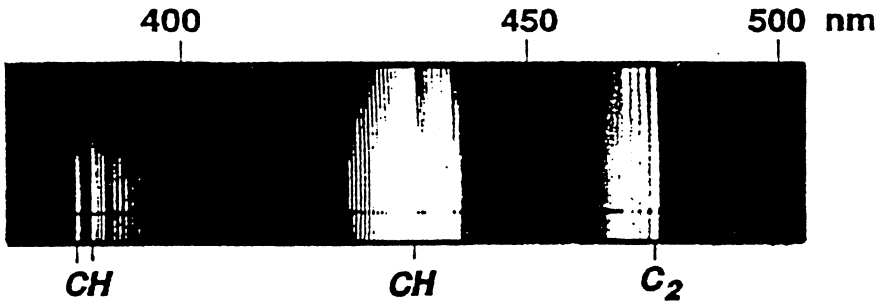

Fig 24: Band spectrum containing lines of CH and C_2; adapted from Gaydon [1974]

Continuous spectra are associated, for example, with the temperature radiation of particles, but may also appear during processes like dissociation or ionization. The continuity of spectra caused by dissociation and ionization results from the fact that one of the energy levels involved is not discrete since the participating particles may store energy by simple translational movement. Therefore no single lines can appear in the spectrum.

In order to determine concentrations and temperatures in elevated temperature systems and technical processes, line and band spectra generally yield the information. However, the radiation of continuous spectra shold not be neglected, since it may in some cases account for disturbing background light.

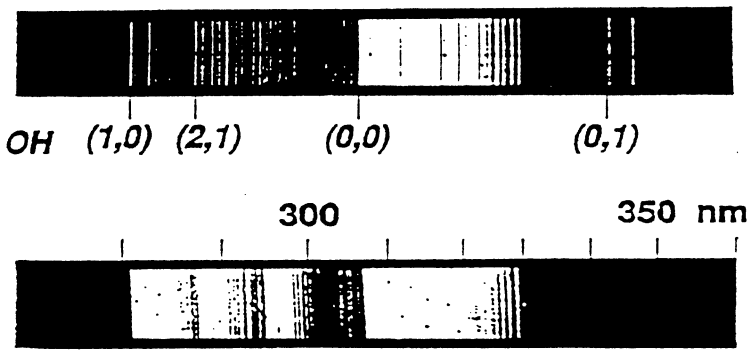

Fig 25: Band spectra of a H_2/O diffusion flame (top) and a H/air diffusion flame (bottom). The (0,0) band, accounting for emissions without a change of the vibrational energy level, is by far the most intensive band. The (1,0), (2,1) bands and the (3,1) band [right of the (2,1) band, not marked] can clearly be seen, showing about equal intensity. Note also that in this part of the spectrum there is no major difference in the appearance between the combustion with air and with O_2. (Adapted from Gaydon [1974])

In fast chemical reactions the emissions of free radicals such as CH, CN, C_2, NH and in most cases OH are of main interest. Especially during the combustion of hydrogen OH is the major radical for emission yielding the desired information. Generally, in self fluorescence only the ground and the first excited electronic state are taken into account, since even in very hot environments the natural population of higher electronic levels is negligibly small. In spectroscopy therefore only two designators are needed to account for the levels involved: the starting, upper level is denoted by a single upper rigth hand index bar

(′), the ending, lower level by double bars (″). For the OH radical the ground level is charcterized by the molecular $X^2\Pi$ configuration, the upper level by the $A^2\Sigma^+$ configuration. Figure 25 shows the spectral range of the strongest OH emissions, which is free of interference from other species. The strongest band by far is the $(v', v'') = (0,0)$ band, meaning there is no vibrational transition coupled with the electronic transition. If the $(0,0)$ band is resolved spectrally, lines resulting from specific rotational transitions can be seen (Figure 26). According to the selection rules only three rotational transitions (J', J'') are possible: $\Delta J = 0$ (Q-branch), $\Delta J = +1$ (P-branch) and $\Delta J = -1$ (R-branch). Due to the electronic spin of the OH radical doublets appear, resulting in two separate lines for each branch which are positioned very close to one another because of the low energy difference between the associated doublet states. The transitions of highest probability for the OH-radical, and therefore highest intensity in the spectrum, are transitions without a change in electronic spin. Transitions within the higher energy doublet state are denoted by a lower right hand index value of '1', those within the lower doublet state by '2'. Therefore six branch-bands appear in each vibrational band: P_1, P_2, Q_1, Q_2, R_1 and R_2. In order to characterize a specific spectral line the associated branch-band and the quantum number of the rotational level of the lower state (J'') are necessary. For example, a transition within the higher doublet state from the rotational level $J' = 10$ to the level $J'' = 9$ is fully specified by the notation $R_1(9)$. An extensive table of energy terms as well as transition probabilities of lines observed in the spectrum is given by Dieke and Crosswhite [1962].

If self fluorescence is applied to get overall information about the reaction process, this is usually done by simple photography or moving pictures. In many cases optical filters are used to select certain band paths for transmission before the sensitive film or receiver is exposed. By this the emissions of specific species and transition bands can be selected from the broadband stray light.

The main parameter needed for the evaluation of the pictures obtained is the rate of spontaneous emissions in the observed wavelength. This rate, ER_{SF}, is given in units of photons per volume and second $(cm^{-3}s^{-1})$ and consists of several factors:

- the total number of molecules per unit volume N
- the mole fraction of the emitting species, given as the relative, partial pressure (i.e. $[OH]$)
- the cumulated transition probability (relative) of all transitions producing emissions in the spectral band $P_t(\lambda)$
- the number of molecules in the upper level of the species, expressed by the exponential term $exp(\frac{-E'}{kT})$. In this term E' is the term energy of the upper level of the regarded particle, k is the Boltzmann constant and T the absolute temperature of the system.

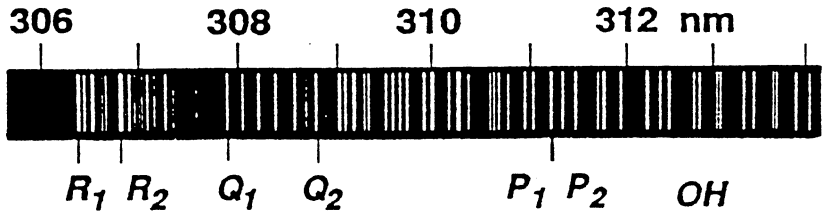

Fig 26: Highly resolved spectrum of the OH - (0,0)-band; the lines result from different rotational transitions within the band. Due to the molecular configuration each branch (P, Q and R) appears in doublets, denoted by lower right hand index numbers. (Adapted from Gaydon [1974])

This yields for the relative fluorescence rate

$$ER_{SF} = N \cdot [OH] \cdot P_t(\lambda) \cdot e^{(\frac{-E'}{kT})} \tag{19}$$

The total number of molecules per unit volume can be approximated in constant pressure systems by the relation

$$N = N_L \cdot \frac{273}{T} \tag{20}$$

with the Loschmidt number

$$N_L = 6.02 \cdot 10^{19} cm^{-3} \tag{21}$$

relative transition probability [-]

v' \ v''	0	1	2	3
0	1,000	0,004	0,000	0,000
1	0,348	0,580	0,003	0,001
2	0,067	0,526	0,289	0,442
3	0,022	0,185	0,543	0,106

band head [nm]

v' \ v''	0	1	2	3
0	306,4	342,8	—	—
1	281,1	312,2	348,5	—
2	260,9	287,5	318,5	325,4
3	244,4	267,7	294,5	302,2

Fig 27: Relative transition probabilites of the vibrational bands of OH; the values are based on the transition probability of the stronges band, the (0,0)-band. On the right the wavelenth of each band head is given. (Adapted from Gaydon [1974])

The relative transition probabilities $P_t(\lambda)$ of the vibrational bands of OH as well as the wavelength of their band heads are given in table 27. In the OH-radical the band heads appear at the lowest wavelengths within the band, their upper rotational transitions are shifted to the red. The transition probability is a number yielding the intensity of a transition in dependence of the total number of molecules in the initial state. The distribution of molecules among the initial states is given by the Maxwell-Boltzmann statistics leading to the exponential term in equation 19. The distribution is a function of the energy content of each state which are constant numbers for any given species. However, there is also a strong temperature dependence of the population distribution.

Again, the most widely used radical OH will be used as an example. In order to calculate the energy E'' of the vibrational levels v' in the upper electronic state $^2\Sigma^+$ the following expression, representing a slight approximation, is used:

$$E' = T'_e + (\frac{1}{2} + v')\omega'_e \tag{22}$$

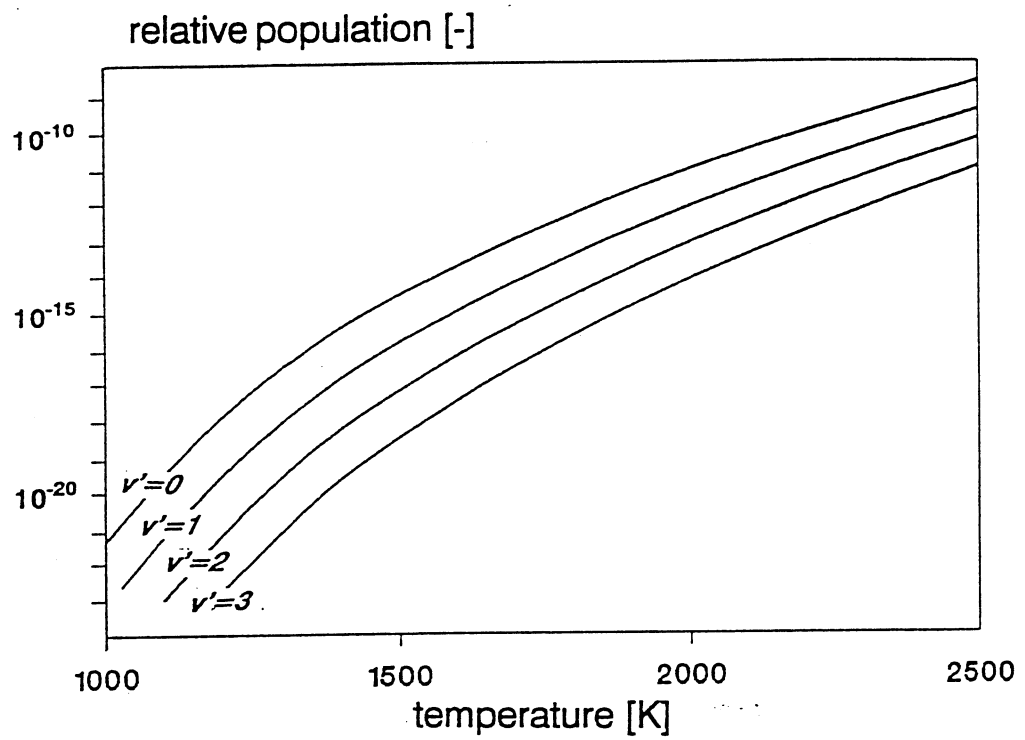

Fig 28: Relative population of the vibrational levels in the $^2\Sigma^+$ upper electronic level of OH as a function of temperature.

The data for the state energy is taken from Huber [1979]:

$T'_e = 32684.1cm^{-1}; \omega'_e = 3178.8cm^{-1}$.

Considering that the relative intensity yield of a transition results from the product of the population and the transition probability, only the lower vibrational levels have to be taken into account. Figure 28 shows the population distribution of the molecules among the first four vibrational states in the $^2\Sigma^+$ term for temperatures from 1000 to 2500 K. It can be seen that at any temperature the difference in population of two neighboring vibrational states is roughly one order of magnitude, decreasing with increasing temperature. If an exposure is made, for example, with a broadband filter letting the entire OH emission pass onto the plate, by far the most radiation results from the $(0,0)$-band. Even at a temperature of 2500 K the two strongest bands beside the $(0,0)$-band, the $(1,0)$ and the $(1,1)$-bands, would account for less than 15%:

$$\frac{ER_{SF}(1,0) + ER_{SF}(1,1)}{ER_{SF}(0,0) + ER_{SF}(1,0) + ER_{SF}(1,1)} = 0,13 \tag{23}$$

However, it is usually possible to select a narrow band pass filter allowing only a small spectral section to expose the sensor. In the case of the OH radical a suitable filter would be an interference filter with a central wavelength of 308 nm and a bandwidth (FWHM) of 10 nm. As can be seen from Figure 25, only the most intensive parts of all three (P,Q,R) branches of the $(0,0)$-band fall in this wavelength range. Therefore there is no influence of the emissions from other bands. The energy E' in the exponential term

of equation 19 may now be taken as a constant and the intensity of the emission is only a function of the concentration of OH and the temperature. Equation 19 yields

$$ER_{SF} \sim \frac{1}{T} \cdot [OH] \cdot e^{\frac{const.}{T}} \tag{24}$$

with

$$const. = -\frac{E}{k} = -49400\ K^{-1} \tag{25}$$

In order to obtain temperatures from self fluorescence, the emissions from two different energy levels have to be evaluated with regard to their intensity of appearance. On the basis of equilibrium thermal distribution, following Boltzmann statistics, the intensity ratios of two selected rotational transition lines can be calculated according to equation 19. However, since now specific, single rotational lines have to be taken into account rather than vibrational bands, their precise rotational energy levels have to be introduced for the energy term $E'(T'_e, v', J')$. The measurement of temperatures on the basis of self fluorescence has been largely replaced by the more exact methods employing laser light sources for stimulation. Since the physical effects concerning molecular distributions and also the evaluation of the line intensities obtained are very similar to the laser light scattering methods, the corresponding formulae for application with self fluorescence can easily be derived from those given in the sections on Raman scattering and Laser Induced Fluorescence. A comprehensive description of temperature determination by self fluorescence is also found in e.g. Dieke and Crosswhite [1962].

When measurements of self fluorescence are taken several effects influencing the observed radiation have to be considered Gaydon [1974]:

- chemoluminescence
- candoluminescence
- self absorption

Each effect shall be shortly characterized in the following paragraphs. Chemoluminescence appears when a certain chemical reaction in a chain of reactions mainly produces molecules in an electronically excited level. These molecules undergo transitions from the higher to the lower electronic energy level just like thermally excited molecules. However, since there is a strong surplus of radiating molecules, equation 19 is no longer valid. Qualitatively the resulting emisions are proportional to the production rate of the species, i.e. OH, rather than related to the species concentration and temperature. Therefore, in systems with high rates of chemoluminescence the emissions clearly mark the production zones of the radicals, i.e. the reaction zones in combustion systems. In hydrogen combustion recent investigations performed by the authors seem to indicate that chemoluminescence rather than thermal fluorescence is the predominant source of emission. For other combustion systems the major emission source should be determined before the application of self fluorecence.

Candoluminescence mainly appears in connection with solid particles in flames with a high hydrogen content. The effect results from a catalytic recombination reaction of H atoms and appears in a continuous band. The spectral position of the band depends on the catalyst. Due to the continuous nature of candoluminescence it should be readily recognizable in an experimental setup and should be avoided wherever possible.

A rather important effect is self absorption. The radiation emitted from a certain location in the investigated volume passes through other areas in which the same species is present. Since the wavelength of the emitted light corresponds exactly to a possible excitation transition of molecules of the same species

in the electronic ground level, there is a high rate of 're'-absorption, called self absorption. This self absorption has two effects: on the one hand the recorded emission intensity from the original point of emission is lower than the actual emission; on the other hand, the re-emission of the 'self-absorbed' light yields a higher emission intensity than would correspond to the actual local concentration and temperature.

These three interference effects are mainly important if very detailed investigations are intended. In order to get an overall picture of the events in the system investigated, they generally need not be regarded, since the effects are well below the basic, thermally caused self emission.

5.2. Experimental Setup and Examples of applications

Self fluorescence technique is mainly used to attain insight into the overall structure and behaviour of fast reaction systems like combustion processes, by investigation of the characteristic radiation emitted from intermediate reaction products. The first step is the selection of the species to be observed, the second step the selection of the spectral region. Useful tools for these primary steps are tables of the emission characteristics which can be found for example in Gaydon [1974]. Helpful is also a full spectrum of the flame in the actual environment. This may be obtained by means of a scan of a spectrograph, recording the intensities as a function of the wavelength either with a photomultiplier or multi-channel cameras.

For the determination of the time resolved location of reaction fronts in flames, the (0,0)-band of the OH radical has proven very valuable. OH appears in rather large quantities in most flames with emission in the UV, therefore showing little or no interference with emissions of other molecules. In addition, OH is really only an intermediate product of combustion, therefore the location of the actual reaction zone can be visualized very well. Species like S_2, CO_2 or H_2O are suitable for (complementary) measurements in the hot, highly emissive post-combustion zone. The selection of the most suitable species depends on the reactants of the process, the environment, temperature and pressure and there are no general guidelines. In any case sufficient emission from the species has to be provided for the measurements.

For experimental setup many combinations of components available may be used. Simple systems consist of three general devices:

- lens assembly
- spectral selection
- sensor

The simplest device, combinig these devices, is a standard photo-camera. The spectral selection, if no special filter is used, is given by the lens and the spectral characteristics of the film (sensor).

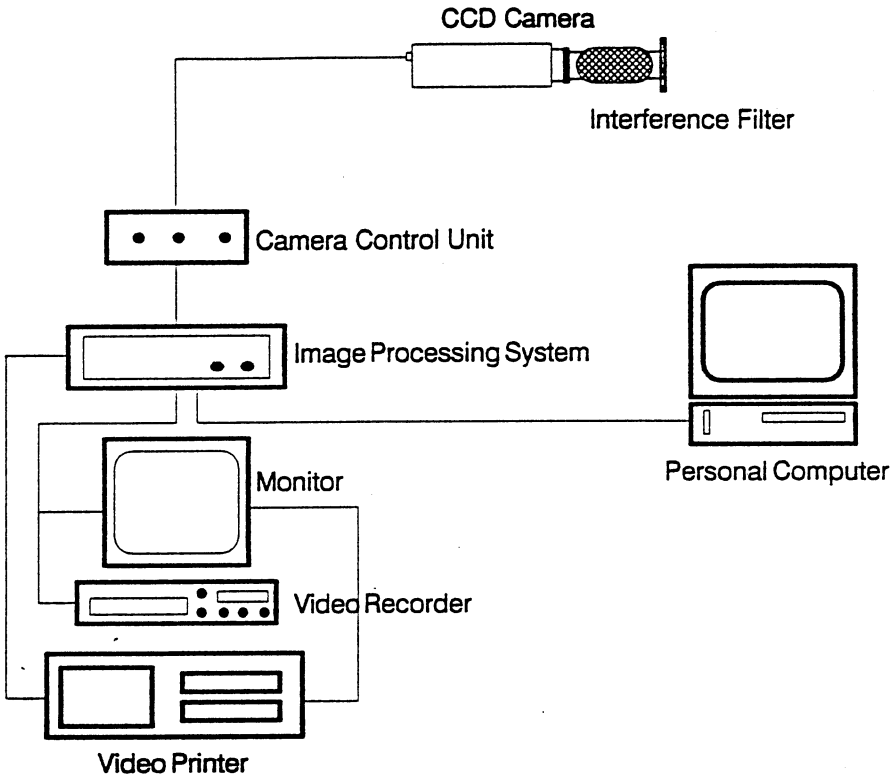

Fig 29: Schematic of setup used for two dimensional viewing of self fluorescence in hydrogen combustion processes Haibel [1993].

In more sophisticated systems, partially adapted to the process investigated, two more basic devices are added:

- system control
- data acquisition, processing and storage

The system described in the following paragraphs represents a typical, at the same time simple, yet very versatile arrangement for the observation of overall events in stationary and unstationary combustion processes. Figure 29 schows the setup schematically. It consist of a standard camera lens, an interference filter, an intensified CCD video camera with controller and an image processing system for data handling. This system consists of a central processing unit connected to a standard VCR, monitor, PC and video printer.

The main part of the setup is the intensified camera. The image intensifier has three important effects on the performance of the camera:

- gateability
- increase in sensitivity
- spectral shift of maximum sensitivity

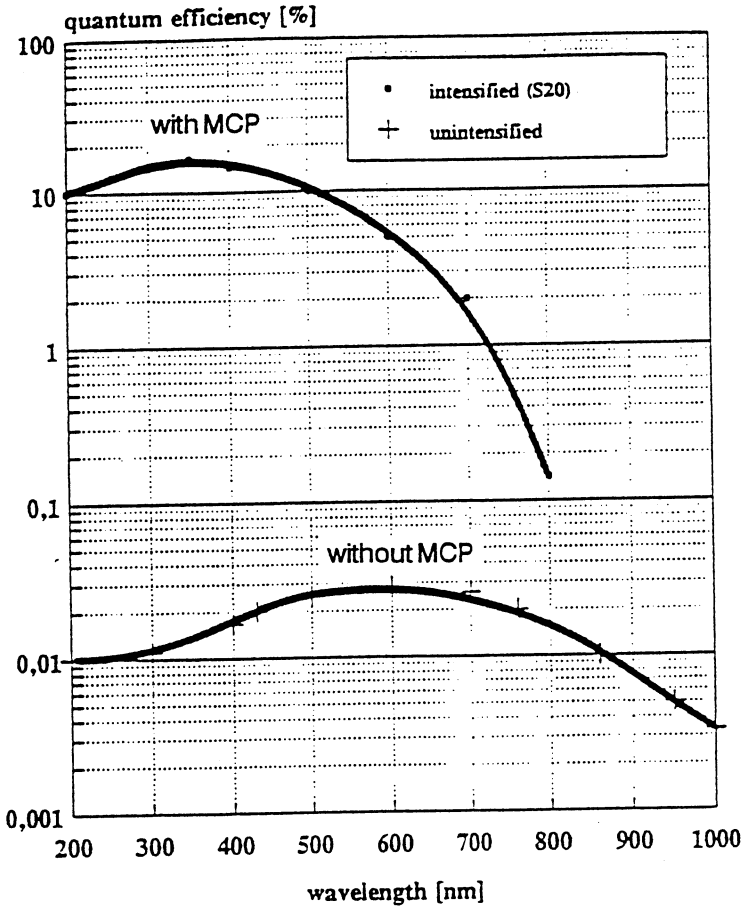

Fig 30: Comparison of the spectral sensitivity and quantum efficiency between standard CCD camera and camera with image intensifier (MCP).

Figure 30 shows the characteristic spectral response curves of two cameras, one with and one without an image intensifier. Beside the tremendous increase in sensitivity, the shift in wavelength of the peak sensitivity from the visible/red region of the spectrum to the UV is important. In the vicinity around 310 nm, where the peak intensity of the OH emissions appear, the increase in sensitivity reaches three full orders of magnitude. This increase in sensitivity is especially important in combination with the second advantageous feature of the image intensifier, the gateability. It is possible to set the shutter speed, i.e. exposure time, to any value between 100 ns and 14 ms. This is very valuable both for investigations of unstationary flame propagation and the capture of fluctuation processes in stationary flames. The camera is equipped with a commercially available UV lens with a focal length of 105 mm. The transmission curve of the lens is shown in Figure 31.

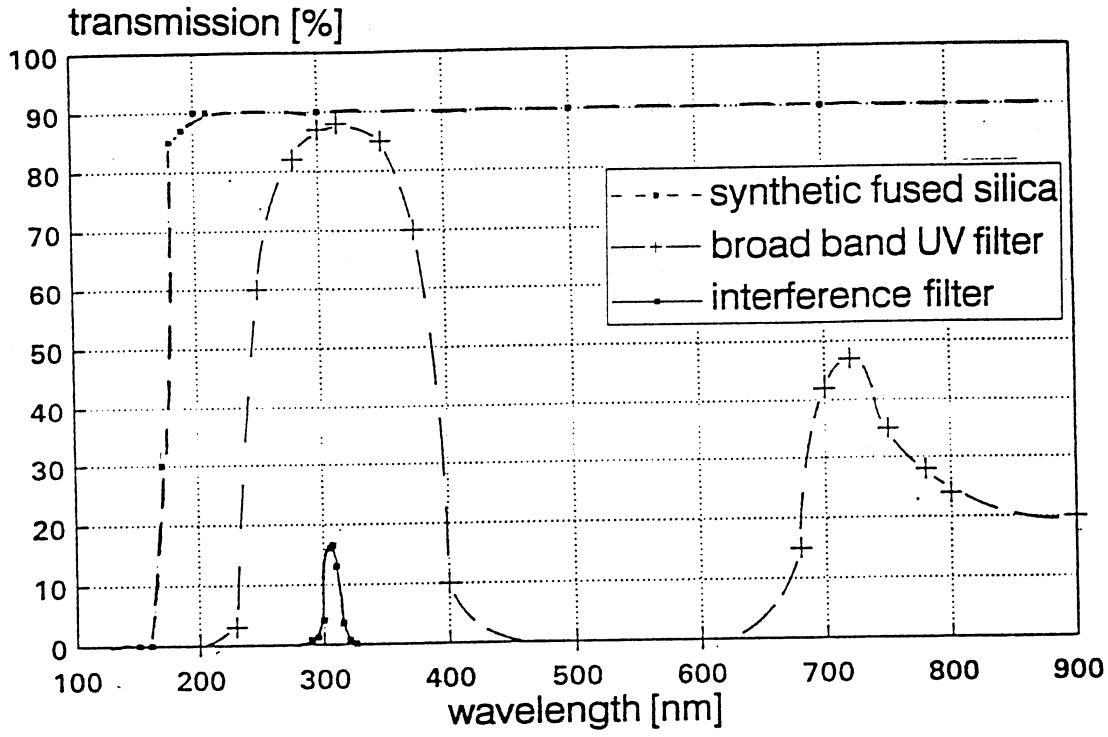

Fig 31: Transmission curves of a) synthetic fused silica, b) broadband UV filter, c) interference filter ($\lambda_c = 307.4\ nm, \Delta\lambda = 10\ nm$).

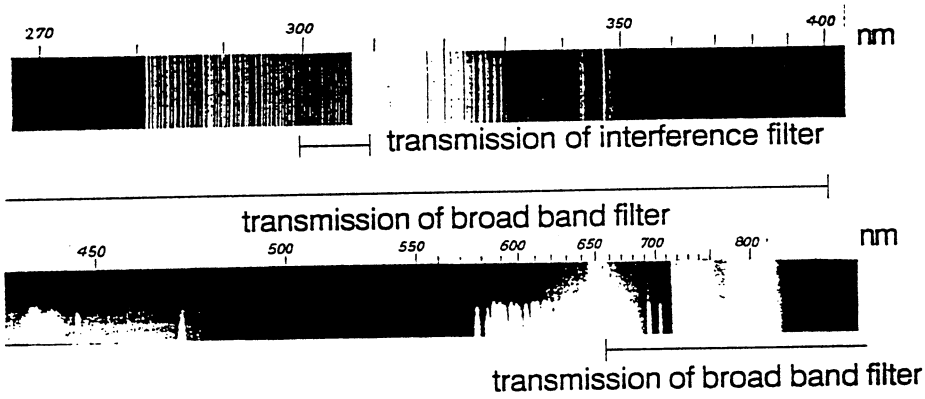

Fig 32: Emission spectrum of a hydrogen-oxygen flame with spectral transmission range of the filters from Figure 30.

Since the system is designed for two dimensional pictures, spectral selection can only be done by optical filters. Very suitable are narrow band pass filters such as interference filters. Interference filters are available for almost any centre wavelength with a choice of different bandwidths. The main disadvantage of interference filters (in the UV) is the comparatively low transmission at the centre wavelength. In the case of the filter used for the described system (centre wavelength $\lambda = 307.4\ nm$; bandwith $\Delta\lambda = 10$ nm) the maximum transmission is only 17% (see Figure 31). A broadband UV (gelatine) filter supplied with the lens has a transmission of nearly 90% around 300 nm. However, the bandwith is very wide (250 - 400 nm) and there is an additional range of transmission in the red/near infrared region in which the emissions of H_2O and O_2 appear (fig. 23). The best filter to be selected depends mainly on the experiments and the environment. For example, in a natural environment the broadband filter permits a large part of daylight to hit the sensor, allowing high background noise and therefore making measurements invaluable.

The light passing the filter is projected onto the sensitive chip with an array of 768x493 pixels and

the intensity recorded by each pixel is read out at the standard (German) video rate of 50 Hz with 8-bit dynamics (256 intensity values). This data is transferred to the central image processing unit and stored there digitally. In this unit simple image enhancement tasks like false color imaging, contrast enhancement etc. may be performed online at the 50 Hz rate. For more sophisticated processing routines single images may be passed on to a PC. If continuous sequences of pictures are desired, the enhanced signal may be passed on directly to a VCR. A high-resolution monitor and a video printer are also provided in the system for visualization and hard copies of the images.

The whole system can be coupled to the processes to be investigated by highly precise timing devices. With this option specific, reproducible effects may be captured instantly. Also, in the timing the system makes a synchronous use of several systems possible, offering a large variety of performances such as the better capture of three-dimensional processes.

Technical heating systems based on combustion, like those in power plants or house furnaces, as well as continuous working engines like gas turbines and ram jets, are basically stationary combustion systems. However, these processes are superimposed by dynamic processes. Typical effects of these dynamic influences are flame instabilities and combustion-induced vibrations.

The possibility of taking pictures at very high shutter speeds makes sophisticated optical probes based on self fluorescence very valuable for investigations of dynamic effects in stationary flames. The simplicity of the optical setup makes applications even in highly complex experimental setups suitable.

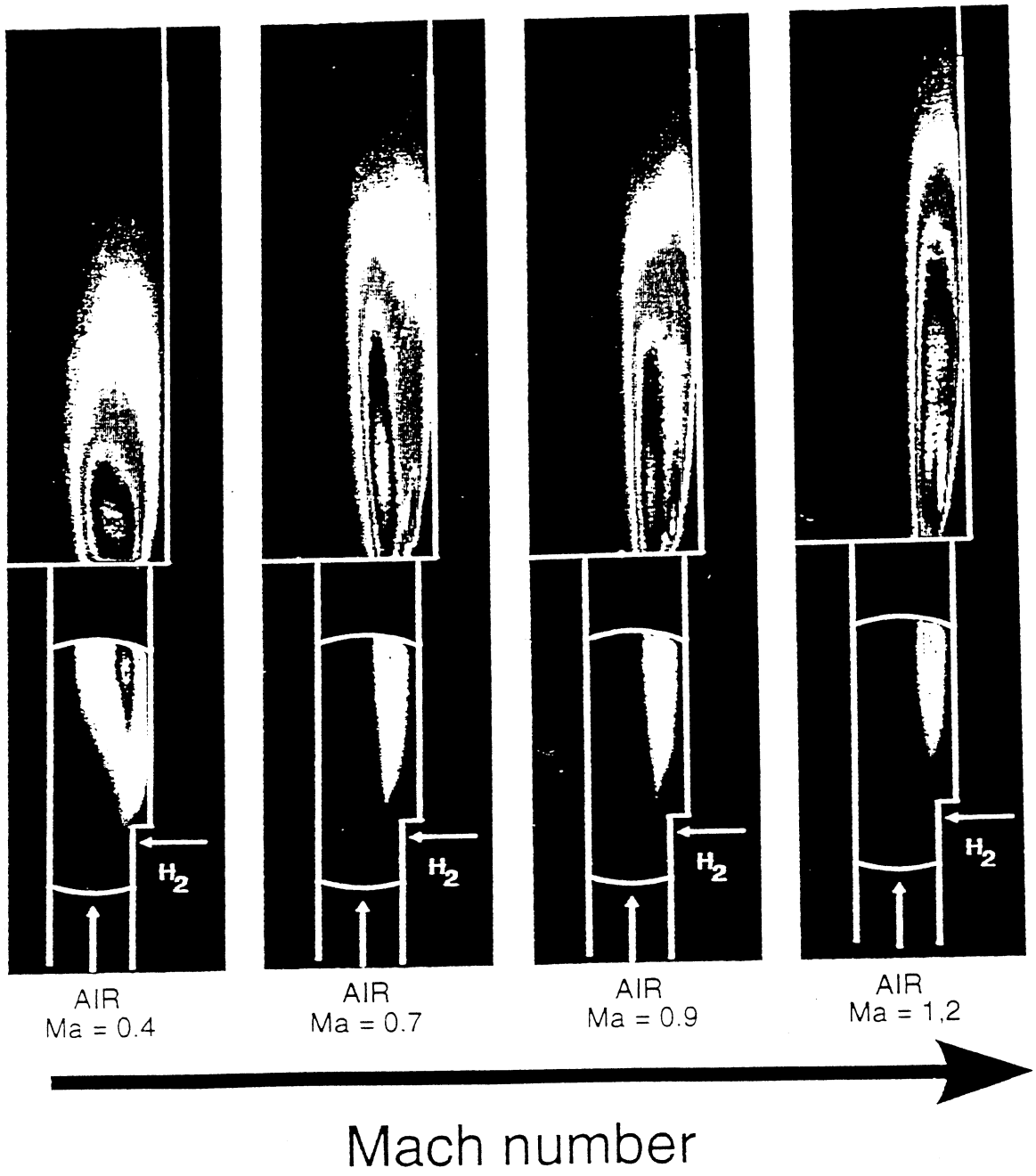

Fig 33: False colour images of the OH-intensity in hydrogen-air diffusion flames in sub- and supersonic main air flows, stabilized behind rearward facing steps. The hydrogen is injected perpendicular to the air flow, as indicated. The shutter speed was set to 1 ms. Haibel [1993]

Figure 33 shows the images of the flames at main stream Mach numbers of 0.35, 0.7, 0.85 and 1.3, stabilized in the recirculation zones evolving from rearward facing steps. The hydrogen was injected from the wall just ahead of the first step at constant mass flow and perpendicular to the air stream. With increasing Mach number the flames become thinner and slightly longer, as would be expected. Remarkable, however, are smaller secondary zones of intensive reaction activity appearing behind the second rearward facing step. These secondary reaction zones can be explained by an additional recirculation zone induced by the second step. In addition, with the aid of the self fluorescence measurements the stabilization point of the flame can be localized; it is always in the free turbulent shear layer separating the main flow and the recirculation zone behind the first step (Haibel [1992]).

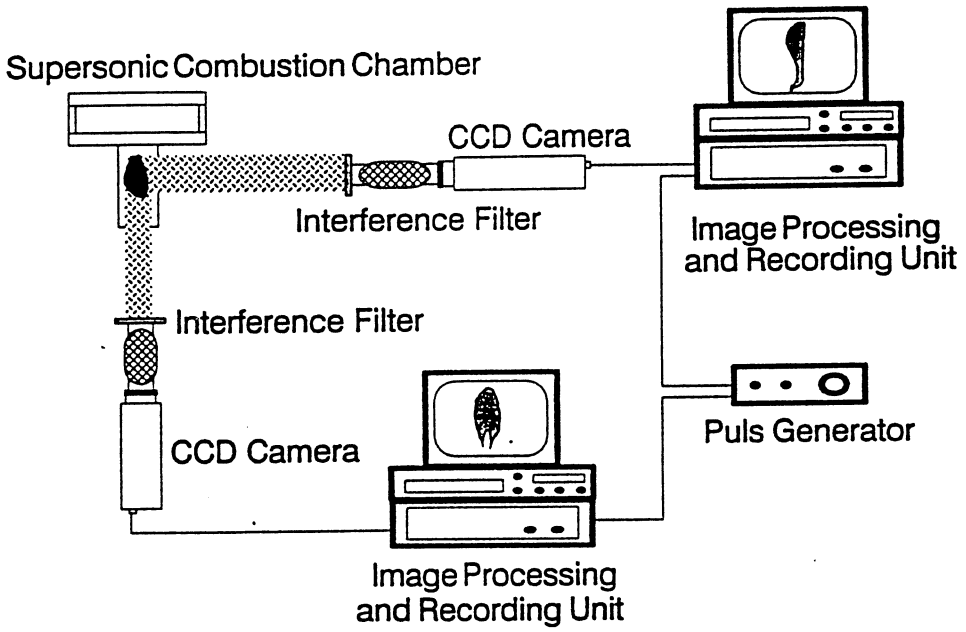

Fig 34: Schematic of setup of cameras for self fluorescence investigations of high speed flames, observed from two directions. A timing device is used to synchronize the two cameras. Haibel [1993]

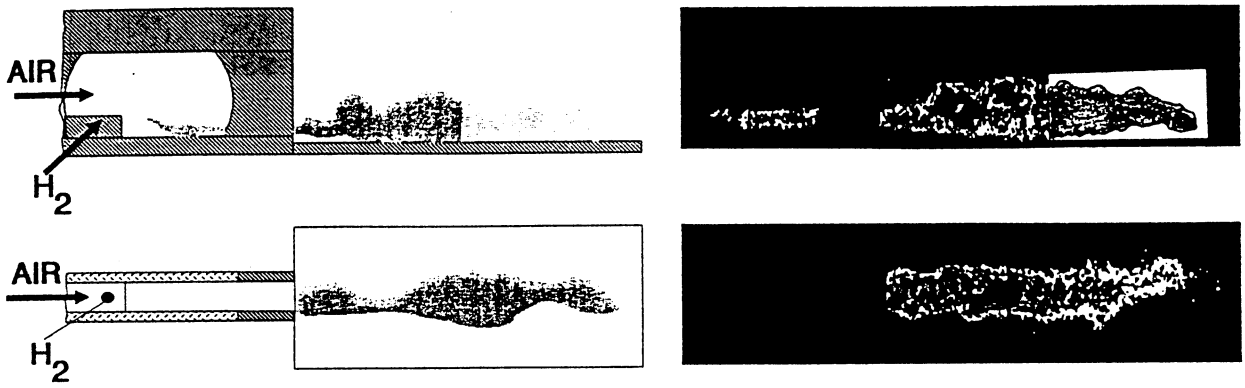

Fig 35: False colour images of flames at a main flow Mach number of 0.8. Both images show the flame at the same instant of time at perpendicular directions of observation. The shutter speed was reduced to 50 μs (Haibel [1992]).

If the flames are looked at from perpendicular directions, more insight into the processes involved can be obtained. Figure 34 shows a schematic of the setup used. Both cameras are synchronized by a timing device in order to record the images at the same instant of time. The shutter speed was reduced to 10 μs. While the images in fig. 33 show a time averaged image due to the long exposure time, the images in fig. 35 reveal the dynamic structure of the flame.

6. Laser induced Fluorescence

Laser induced Fluorescence (LIF) methods are generally applicable to a large number of species. Due to its large signal intensities and the high achievable spatial resolution, the main field of application of LIF is the two-dimensional imaging of reacting flows. Here the intermediate products formed in the separate steps of the overall reaction process and residuals appearing with rather low concentrations are of main interest. With the rising importance of environmental aspects in all fields of propulsion systems, energy consumption and emission of pollutants the detectability of low concentration species will be in great

demand. LIF methods provide powerful tools for monitoring these type of species.

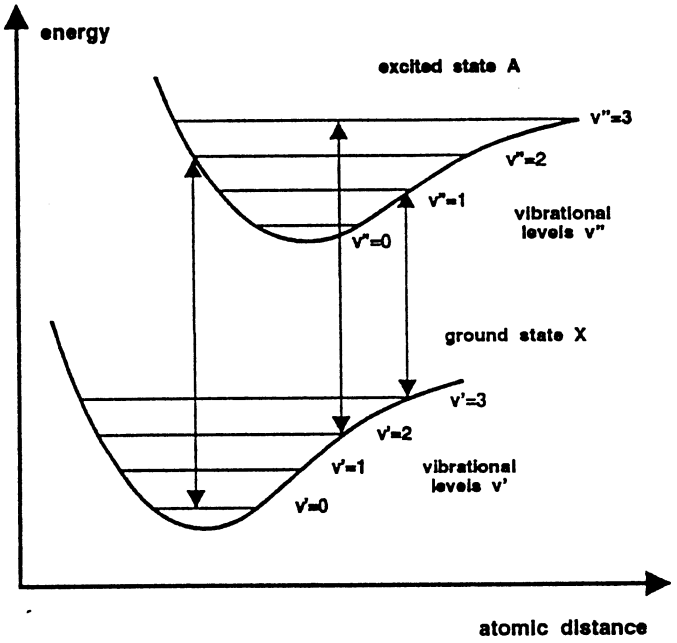

Fig 36: Energy diagram of electronic levels and their vibrational levels. The rotational levels within each vibrational level are not shown in this schema, although they do play an important role in LIF thermometry measurements. For more details on the rotational and vibrational structure of molecules, chapter 6 should be consulted. Each potential curve exhibits a specific minimum indicating its stability. The spacing of the atoms in the molecule during the vibrational movement varies between the intersections of the line of the vibrational level and the potential curve. According to the Franck-Condon principle, transitions from the end points are more intense than from the middle of vibrational lines.

NOMENCLATURE

A	first Einstein coefficient
B	second Einstein
B	rotational constant
c	speed of light
E	energy
FR	fluorescence rate
g	statistical weight factor
h	Plancks constant
I	intensity
J	rotational quantum number
k	Boltzmann constant
N	number density of molecules
P	rate of predissociation
Q	partition function
Q	rate of quenching transitions
T	absolute temperature in thermodynamic equilibrium
T	term energy
t	time
V	observed volume
v	quantum number
γ	mole fraction
λ	wavelength
η	efficiency
ν	frequency of light
$\Delta\tilde{\nu}$	laser band width
σ	collosional cross section
Ω	solid angle of collecting optics
ω_e	vibrational constant

SUBSCRIPTS

e	electronic term
i	counting variable
J	rotational Energy level
j	counting variable
L	Loschmidt
lin	linear LIF
pre	predissiciation LIF

S	regarded species
v	vibrational energy level
rot	rotational states
sat	saturated LIF
tot	refering to all species
vib	vibrational states
ν	spectral function
0	laser light
1	lower energy state
2	upper energy state

6.1. Basic Principles of Laser Induced Fluorescence

Before the physical processes involved in LIF measurements are discussed, the simplified energy level model of molecules presented in chapter 6 of this paper is outlined. It is depicted in simplified form in Figure 36 and shows two electronic energy levels with their inherent vibrational levels. Generally the lower energy level regarded is the ground electronic state designated by the letter X; only this state is considerably populated. The upper level here is designated by the letter A, i.e. the first excited state . However, in other cases this may well be a different state $(B, C, ...)$. The total energy content E_{tot} in units of $[cm^{-1}]$ of a molecule in the electronic level e (X, A, ...), the vibrational level v (0, 1, ...) and the rotational level J (0, 1, ...) are approximately given by

$$E_{tot} = E_e + E_v + E_J = T_e + \omega(v + \frac{1}{2}) + BJ(J+1) \tag{26}$$

The constant values for the term energies T_e as well as the vibrational and rotational constants, ω and B respectively, of the regarded electronic level can be found in e.g. Huber/Herzberg [1979].

Generally, fluorescence is a transition from an upper to a lower energy level in conjunction with a spontaneous emission of a photon. The energy of the photon is equal to the energy difference of the two levels involved. According to Planck's law

$$E = h\nu \tag{27}$$

this energy is directly proportional to the frequency of the emitted light. Transitions within the electronic ground state involve low energy differences and therefore appear in the infra-red region of the electromagnetic spectrum. Transitions between electronic states, on the other hand, are generally associated with emission frequencies in the visible (green or blue) or the UV region.

Due to the poor population of excited states even at high temperatures (the population of the A state of OH at $T = 2500$ K is roughly nine orders lower than the population of the ground state X), the reverse process of emission, namely absorption, is used to efficiently populate the upper electronic level and obtain higher signal strength. Typical lifetimes, meaning the time the molecule stays in the upper electronic level, are of the order of 10^{-8} s. For molecules in the excited electronic levels there are different subsequent processes possible, shown schematically in the energy level diagram of Figure 37:

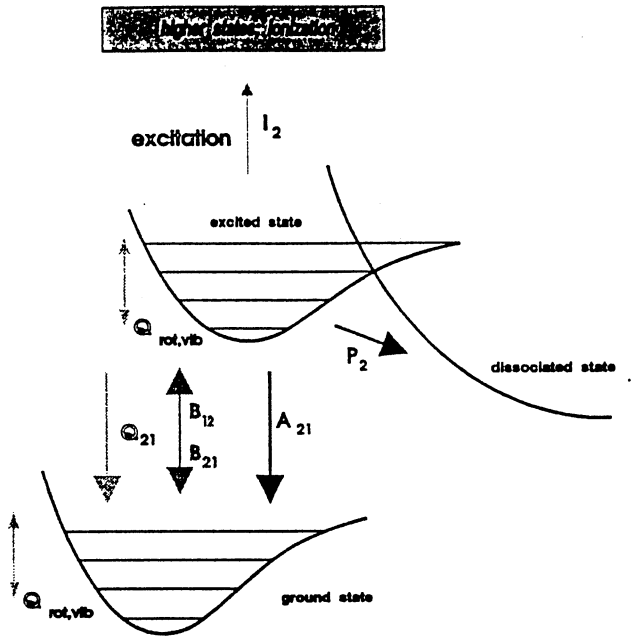

Fig 37: Possible events for a molecule in the upper electronic state specified by the rate coefficients used in the equations. The intermolecular collisional quenching rate Q_{21} includes processes involving two electronic states. Those involving only ro-vibronic levels within the same electronic state are denoted by $Q_{rot,vib}$. The fluorescence transitions A_{21} do not necessarily occur between the identical ro-vibronic levels involved in the laser excitation process, but rather follow the 'natural' transition probabilities determined by the Franck-Condon selection rules. The laser-stimulated processes between the regarded states E_1 and E_2 are determined by the Einstein coefficient B in both directions B_{12} and B_{21}, which are coupled by the degeneracies g_J of the corresponding energy levels. Processes leading to ionization are denoted by I_2. The actual transition rate is obtained by multiplying the Einstein coefficient by the spectral intensity of the laser. For some molecules the potential curves of stable upper electronic states have an intersection point with an unstable electronic state (repulsive molecular configuration without minimum in potential curve) leading to dissociation of the molecule. A stable state which is coupled to a state leading to dissociation is called 'predissociated' state and the rate of dissociation is expressed by P_2.

- the molecule can undergo a laser-stimulated transition back to the ground state (emitting a photon of light at the laser frequency in the direction of the laser beam)
- the molecule can absorb an additional photon of the incident light and go to an even higher energy level (including ionization)
- collisions of the molecules with other molecules may cause a transition to a lower energy state without emission of light; this effect is referred to as 'collisional quenching'
- interactions within the molecule may lead to dissociation; if the dissociation caused by a shift from a stable configuration to an unstable electronic configuration (showing a repulsive energy potential curve without specific energy minimum), the process is called 'predissociation'
- the molecule undergoes a fluorescence transition to the ground electronic state involving light emission
- collisions with other molecules may cause vibrational and rotational transitions within the excited state with subsequent fluorescence

Since time scales of these processes are of vital importance for interpretation of the actually observed intensity of fluorescence, the time dependent equation of the population of the different energy levels involved has to be established. The population $N_j(t)$ of a specific energy level j as a subset of the set of

levels i is defined by the differential equation

$$\frac{dN_j(t)}{dt} = \sum_{i \neq j} N_i(t) R_{ij} - N_j(t) \sum_{i \neq j} R_{ji} \tag{28}$$

where R_{ij} is the integral rate coefficient in units of $[s^{-1}]$ for all processes yielding an increase in the population of the level j, and R_{ji} which in analogy represents all processes depopulating the level j.

If the regarded set of energy levels E_i is reduced to two levels E_1, E_2, coupled by the energy content of a photon of monochromatic radiation of the corresponding frequency ν_{21}

$$\Delta E_j = E_2 - E_1 = h\nu_{21} \tag{29}$$

with j=2 as the upper level, equation 28 yields

$$\frac{dN_2(t)}{dt} = N_1(t) R_{12} - N_2(t) R_{21} \tag{30}$$

If the integral coefficients R are explicitly stated, equation 30 extends to

$$\frac{dN_2(t)}{dt} = N_1(t)[B_{12} I_\nu] - N_2(t)[Q_{21} + B_{21} I_\nu + A_{21} + I_2 + P_2] \tag{31}$$

The coefficients Q, B, A, P and I appear in place of the coefficient R. Collisional excitation Q_{12} is usually negligible. Since the photo-ionization rate is usually comparatively small, this term shall be neglected in the following considerations. The rate of pre-dissociation depends mainly on the species investigated, but is nearly independent of the environment. For the following considerations, a non-predissociated species or electronic state shall be regarded (i.e. $P_2 = 0$); the case of pre-dissociation will be discussed separately later. The first Einstein coefficient A_{2f} for a transition from the upper level 2 (in the electronically excited state) to the lower levels f (in the electronic ground state) is equal to the reciprocal value of the characteristic lifetime τ of the excited energy level E_2 of the species s

$$\sum_f A_{2f} = \frac{1}{\tau_{2,s}} \tag{32}$$

where f denotes a state in the lower electronic state. The distribution of the transitions among the lower states f occurs according to the corresponding Franck-Condon factors for the transition. The values of the lifetimes and the Franck-Condon factors again are to be taken from Huber and Herzberg [1979] and Eckbreth [1979].

The second Einstein coefficient B represents laser stimulated processes, both for population and for depopulation. It is coupled to the coefficient A by the frequency of the laser light ν

$$B_{21} = \frac{c^3}{8\pi h} \frac{1}{\nu^3} A_{21} \tag{33}$$

and has to be multiplied by the laser spectral intensity I_ν. This is a function of the laser irradiance I_L at the considered frequency ν of the transition and the spectral bandwidth $\Delta\nu$

$$I_\nu = \frac{2 I_L}{\pi c \Delta\nu} \tag{34}$$

The coefficients B for stimulated population and depopulation are coupled by the degeneracy of the two levels involved

$$g_1 B_{12} = g_2 B_{21} \tag{35}$$

Assuming that the total population $N_1(t) + N_2(t)$ of the two energy states remains constant, and in addition that the laser pulse is long compared to the time constant τ of the solution of the differential equation 31, the system reaches a steady state with

$$N_2(t \gg \tau) = constant = N_1(0)\frac{B_{12}I_\nu}{[B_{12}I_\nu(1 + g_1/g_2) + Q_{21} + A_{21}]} \tag{36}$$

yielding the rate of fluorescence FR

$$FR = A_{21}N_2(t \gg \tau) = A_{21}N_1(0)\frac{B_{12}I_\nu}{[B_{12}I_\nu(1 + g_1/g_2) + Q_{21} + A_{21}]} \tag{37}$$

In order to capture the influence of the spectral intensity of the laser I_ν and the population/depopulation ratio given by the term $(1 + g_1/g_2)$ equation 37 is arranged in the form

$$FR = N_1(0)B_{12}I_\nu\left(\frac{A_{21}}{A_{21} + Q_{21}}\right)\left(\frac{1}{1 + I_\nu/I_\nu^{sat}}\right) \tag{38}$$

The newly introduced term I_ν^{sat} is called the saturation intensity of the laser light and is defined as

$$I_\nu^{sat} = \frac{A_{21} + Q_{21}}{B_{12}(1 + g_1/g_2)} \tag{39}$$

Is the laser intensity well below this saturation limit ($I_\nu \ll I_\nu^{sat}$ or $B_{12}I_\nu \ll Q_{21} + A_{21}$), equation 38 yields

$$FR_{lin} = N_1(0)B_{12}I_\nu\frac{A_{21}}{A_{21} + Q_{21}} \tag{40}$$

This is called the linear fluorescence signal because it is proportional to the laser intensity. The factor $A_{21}/A_{21} + Q_{21}$ is often referred to as the Stern-Vollmer factor. The problems arising from linear LIF are the often unknown rates of the quenching constants Q_{21}, which depend on temperature, pressure and composition of the gas under investigation and are generally significantly higher than the rate of the spontaneous emission A_{21}.

Is the laser intensity well above the saturation level ($I_\nu \gg I_\nu^{sat}$ or $B_{12}I_\nu \gg Q_{21} + A_{21}$), fluorescence becomes independent of Q_{21}. The fluorescence rate for this case is

$$FR_{sat} = N_1(0)\frac{A_{21}}{1 + g_1/g_2} \tag{41}$$

and the technique is often called laser induced saturated fluorescence [LI(S)F]. The assumption that no molecules are lost, i.e. $N_1(t) + N_2(t)$ =constant, holds strictly only for the first excited states of atoms. For molecules, collisions as well as radiation usually leads to other states $i \neq 1, 2$. In this case it has to be assumed that no chemical reactions occur and, secondly, the collisional redistribution is fast enough to maintain Boltzmann equilibrium. In most cases the stationary state is not obtained at the beginning and the end of the laser pulse (time) as well as in the wings of the beam profile (space).

Another possibility to avoid the problems of linear LIF in near atmospheric pressure investigations is the use of the so-called laser induced predissociated fluorescence [LI(P)F]. Here the excitation transition is chosen such that pre-dissociation of the upper state occurs at a high rate and the P term in equation 31 becomes important. Introduction of P_2 in equation 40 yields

$$FR_{pre} = N_1(0)B_{12}I_\nu\frac{A_{21}}{A_{21} + Q_{21} + P_2} \tag{42}$$

The schematics of the potential curves for predissociation and the processes involved in LI(P)F are shown in Figure 37. Usually the predissociation rate P_2 is significantly larger than both the fluorescence rate A_{21} and the quenching rate Q_{21}

$$P_2 \gg Q_{21} \gg A_{21} \tag{43}$$

therefore the proportionality factor for the fluorescence yield becomes approximately

$$\frac{A_{21}}{A_{21} + Q_{21} + P_2} \simeq \frac{A_{21}}{P_2} \tag{44}$$

Although the high predissociation rate significantly decreases the overall fluorescence intensity, the quantitative interpretation of the signals is more accurate. In contrast to LI(S)F, that is based on sufficiently fast redistribution, the effect of collisions is completely eliminated in LI(P)F. In LI(P)F (as well as in LIF and LI(S)F) care has to be taken to avoid depletion of the ground state, because otherwise collisions within the electronic ground state repopulate the level and make the signal sensitive to the gas composition.

Concentration Measurement The concentration of a species is coupled to the fluorescence rate by equation 37. The term related to the concentration is the population of the lower laser-coupled state $N_1(0)$ before the start of the excitation process. In a volume V the number of molecules $N_{S,1}$ of the regarded species S in the energetic state defined by the quantum numbers for vibration v_1 and rotation J_1 is

$$N_{S,1} = \gamma_S N_{tot} V \cdot \left(\frac{g_1(2J_1 + 1)}{Q_{rot} Q_{vib}} \right) \cdot exp\left(-\frac{hcE_1(v, J)}{kT} \right) \tag{45}$$

with γ_S as the mole fraction of the species, N_{tot} the total number density of molecules, $E_1(v, J)$ the molecular energy of the state in $[cm^{-1}]$, k as Boltzmann's constant and T the system temperature in $[K]$. $Q_{rot,vib}$ are the sum of all vibrational and rotational states and are stated explicitly in chapter 6, 'Raman diagnostic'. The total number density of molecules is also dependent on the temperature. Assuming the applicability of the equation for the perfect gas at constant pressure and gas constant of a system, it is inversely proportional to the temperature

$$N_{tot} \simeq N_L \frac{273}{T} \tag{46}$$

where $N_L = 6 \cdot 10^{19} cm^{-3}$ is Loschmidt's number.

The fluorescence signal obtained and processed in an experiment is the number of photons n_{LIF} per second reaching the detector from a considered volume of the measurement field. For the example of the linear fluorescence signal equations 40, 45 and 46 yield

$$n_{LIF} = \left(\eta_c \frac{\Omega}{4\pi} \right) [\gamma_S N_{tot} V \cdot \left(\frac{g_1(2J_1 + 1)}{Q_{rot} Q vib} \right) \cdot exp(\frac{hcE_1(v, J)}{kT})](B_{12} I_\nu \frac{A_{21}}{A_{21} + Q_{21}}) \tag{47}$$

The first factor in equation 47 is necessary to correct for the losses in the collection of the photons. Since the fluorescence photons are emitted into the full solid angle of 4π, only the part covered by the collection solid angle Ω can be captured. The detection efficiency η_c is determined by the arrangement and includes losses at the various elements in the optical path of collection. The number of captured photons can again be converted to energy or intensity values at the detector surface by Planck's law (equation 27).

The difficulties in determining the quenching rates Q_{21} has already been considered above and also applies to equation 47. For LI(S)F and LI(P)F the last factor has to be replaced according to equations 41 and 42 respectively.

For a given setup, apart from the strong influence of quenching effects the signal obtained in a measurement is dependent on the concentration of the species and the temperature. The temperature influence on the population density of the lower laser-coupled state 1 depends primarily on the constants of the molecule under investigation and can be neglected for atoms. In many cases it is possible to find a transition which does not show a strong temperature dependence in the temperature range expected in the experiment. For example, in combustion environments the change in molar species concentration of the intermediate reaction products exhibits much stronger changes than the change in temperature. Therefore the obtained fluorescence signals give a very good qualitative picture of the concentration of these intermediate species, yielding ample information on the location and fluctuations of the reaction zone. In any case, the selection of the excitation levels employed is a very important step in the design of the LIF probe and the conditions of the system under investigation have to be considered.

Temperature Measurement Temperature measurements are possible by either exciting different stimulated transitions and observing the total emissions at a fixed excitation wavelength (excitation method) or observing the spectral distribution of the emissions induced by a fixed transition (fluorescence spectroscopy method).

If the light source can be tuned to stimulate electronic transitions from different single rotational levels within a vibrational level, the observed fluorescence intensity I_{LIF} can be obtained from equation 47. The variables characterizing the experimental setup, i.e. η_c, Ω, I_ν and V, are identical for excitation of spectrally close lower states. Assuming furthermore that the coefficients for emission A_{21} and quenching Q_{21} do not vary with excitation frequency, which is not a really valid assumption, equation 47 can be written in the logarithmic form

$$ln(\frac{I_{LIF}}{B_{12}g_1(2J_1+1)}) = -\frac{hcE_1(v,J)}{kT} + constant \tag{48}$$

and the solution for the temperature becomes

$$T = \frac{hcE_1(v,J)}{k} \cdot -ln(\frac{I_{LIF}}{B_{12}g_1(2J_1+1)}) + constant^{-1} \tag{49}$$

The experimental scanning through the spectral range of transitions of the regarded species usually takes more time than the characteristic timescales of the system under investigation allow without change of the system. Therefore it is very suitable to use two distinct lines for excitation and to compare the broadband fluorescence signals. Assuming a transition from two rotational states a and b (i.e. $J_{1,a}$ and $J_{1,b}$) with $J_{1,a} < J_{1,b}$ from the same vibrational level of the ground state to the same ro-vibronic level v_2, J_2 in the upper electronic state, the following equation evolves

$$\frac{I_{LIF,1}}{I_{LIF,2}} = \frac{B_{12,1}g_{1,a}(2J_{1,a}+1)}{B_{12,2}g_{1,b}(2J_{1,b}+1)} \cdot exp[(\frac{hc(E_1(v,J_{1,b}) - E_1(v,J_{1,a}))}{kT}] \tag{50}$$

This equation, however, is only applicable if the laser spectral intensity and the detection efficiency are equal for both transitions. Otherwise slight modifications of equation 50 have to be done according to equations 35 and 47.

The excitation method requires light sources that are not only tunable but also exhibit very narrow bandwidths in order to avoid simultaneous excitation of several rotational levels in the lower laser-coupled state. Additionally, since fluorescence is often observed in the same spectral range, the lasers and detection devices have to be triggered sequentially, with time delays below the characteristic timescales of the investigated system. Therefore, the fluorescence spectroscopy technique may be advantageous in some applications. In this technique stimulated excitation occurs with a single laser pulse, which in this case may have a wider bandwidth exciting several transitions within a vibrational band. The lifetimes in

the upper electronic state of the molecules undergoing spontaneous emission are assumed to be longer than the time it takes the molecules to reach rotational thermal equilibrium, i.e. a distribution among the rotational levels J_2 according to the Boltzmann equation. Therefore the fluorescence spectrum from the electronically excited state can be analysed for its rotational structure to obtain the temperature. Due to the necessity of thermal equilibrium this method is sometimes referred to as thermally-assisted fluorescence. Equation 47 yields for the fluorescence spectroscopy method with the spontaneous emission rate $A_{21}(J_2)$ from the upper rotational level J_2

$$ln(\frac{I_{LIF}}{A_{21}(J_2)\ g_2\ (2J_2+1)}) = -\frac{hcE_2(v,J)}{kT} + constant \tag{51}$$

The spectral selection of the observed signal has to be very fine to distinguish the different rotational levels. This can be achieved with high resolution spectrometers. For planar applications, however, this is not possible.

Therefore a different strategy for monochromatic fluorescence thermometry has been employed. In the above equations for temperature measurement it was always that the fluorescence from the same location and the same vibrational level of the upper laser-coupled state was used. Therefore the assumption of identical collisional quenching conditions is applicable. If, on the other hand, fluorescence induced by monochromatic light is to be monitored two-dimensionally with one light collection channel, the temperature dependence of collisional quenching Q_{21} has to be taken into account. This technique is called absolute fluorescence because the temperature is obtained from the absolute fluorescence intensity distribution . A simple approach, introduced by Hanson [1990] , to model the collisional quenching coefficient Q_{21}, is

$$Q_{21} = N_{tot}\sigma_c c\bar{v}(T) \tag{52}$$

where σ_c is the collisional cross-section and $c\bar{v}(T)$ is the mean velocity of the molecule as a function of temperature. If the collisional cross-section is taken to be independent from the temperature and the mean molecular velocity is proportional to the square root of the temperature, the factor for collisional quenching becomes

$$Q_{21} \sim N_{tot}T^{1/2} \tag{53}$$

Since in every regarded location the same transition is used, all factors in equation 47 except for the collisional quenching, the exponential expression and the mole fraction of the observed species are constant. Assuming $Q_{21} \gg A_{21}$, equations 27, 47 and 52 give

$$I_{LIF} \sim \gamma_S T^{1/2} exp(\frac{hcE_1(v,J)}{kT}) \tag{54}$$

If the mole fraction γ_S of the regarded species does not change within the observed volume, the obtained fluorescence can be scaled to the temperature very easily with the above equation, needing only one reference point of known temperature . This is also possible in reacting flows, if inert particles are added to the flow and used for LIF.

6.2. Calibration procedures

General remarks As illustrated in chapter 6.1 of this paper the LIPF signal n_{LIF} increases linearly with the number density $N_{S,1}$ of the molecule in the probed quantum state.

$$n_{LIF} = CN_{S,1} \tag{55}$$

In the same way using the two-line approach the temperature is related to the signal ratio $R = I_{LIF,1}/I_{LIF,2}$ by:

$$R = C \exp\left[\frac{hc(E_1(\nu, J_{1,b}) - E_1(\nu, J_{1,a}))}{kT}\right] \tag{56}$$

To convert the measured fluorescence signals to absolute densities or temperatures a calibration has to be performed to determine the constant C. This can be done in several ways. First C can be in principal determined theoretically by calculating all the necessary spectroscopic, optical and detector data such as fluorescence yield, transmission efficiency of the collection optics and conversion efficiency of the image amplifier. Of course in the case of LIF/LIPF measurements this is often very difficult because a deep understanding of spectroscopy is necessary as well as some parameters of the setup which may not be known from a theoretical standpoint like the variation of the sensitivity of the pixels on the CCD.
Therefore the easiest and most reliable way to convert the emission intensities is a calibration measurement. The calibration is a reference measurement of an object, where the temperature and total as well as partial densities are known. Therefore air at S.T.P (standard temperature, pressure) is the easiest reference object. In other cases measurements with independent techniques have to be made to gain all the necessary parameters. Useful approaches are non intrusive techniques such as Rayleigh scattering (for the determination of the total density or the temperature, if the pressure is known) or absorption measurements as well as intrusive concentration measurements with gas analysis instruments or temperature measurements with radiative corrected thermocouples. If special types of burners (like the one-dimensional flat flame burner) are used it is even possible to calculate theoretical concentration and temperature profiles and equilibrium concentrations. In the next chapter it is shown in detail how this can be useful to calibrate concentration measurements of unstable species like the OH radical.
In general the calibration has to be done before or after the actual measurement under identical conditions. Identical conditions means that the same setup is used with the same filters, camera settings, laser parameters etc.. In this way, the calibration procedure yields the relation between the measured signal in counts at the camera and the density or temperature of the corresponding species in the object under study (see equation 55 and 56). Consequently the units of C are [counts x cm3 / molec] in the case of the number density measurements and dimensionless [-] for the temperature determination. The procedure has to be done for each different detection scheme.

Density and concentration Measurements To simulate the conditions of the object under investigation as closely as possible different calibration objects have to be used. For example the simulation of the preheated air streaming through an atmospheric model combustor can be done with a simple hot fan covering a temperature range from 300 K up to 1000 K. With this setup total density calibration for Rayleigh measurements as well as number density calibration of O_2-LIPF signals can be recorded as a function of temperature given by calibrated thermocouples.

For the calibration of other stable molecules like NO, H_2O or gas mixtures at pressures different to one bar a heatable calibration cell is used. A pressure range from 0 to 5 bar at temperatures from 300 to 1100 K can be realized. The cell consists of a 4 way cross made of stainless steel and can be evacuated by a vacuum pump. The absolute pressure in the cell is measured by a pressure transducer and the temperature is determined with two thermocouples located at different positions in the cell. Four silica fused windows with a diameter of 38 mm provide optical access for the laser beam and the detection system.

For the calibration of the concentration measurement of transient molecules in flames like the OH radical we use a one-dimensional flat flame burner (type McKenna), shown in figure 38. The flat flame burner consists of a sintered bronze water cooled burner plate surrounded by a sintered porous shroud

ring for introduction of a shielding gas (nitrogen), both enclosed in a housing assembly with connections for water cooling, premixed fuel/air and shroud gas. The flow rates are measured and controlled to vary the stoichiometry over a wide range. The advantage of this device is that the one-dimensional premixed flame is experimentally well studied and can be treated with theoretical calculations to predict concentration and temperature profiles as well as equilibrium species concentrations. Figure 39 gives an example of a CHEMKIN / PREMIX (Kee, 1980, 1983, 1985, 1987) calculation showing the concentration profile of OH as a function of the height above the burner plate in a premixed H2 /air flame at an equivalance ratio of 1.29 The dashed line in figure 39 shows the corresponding measured profile.

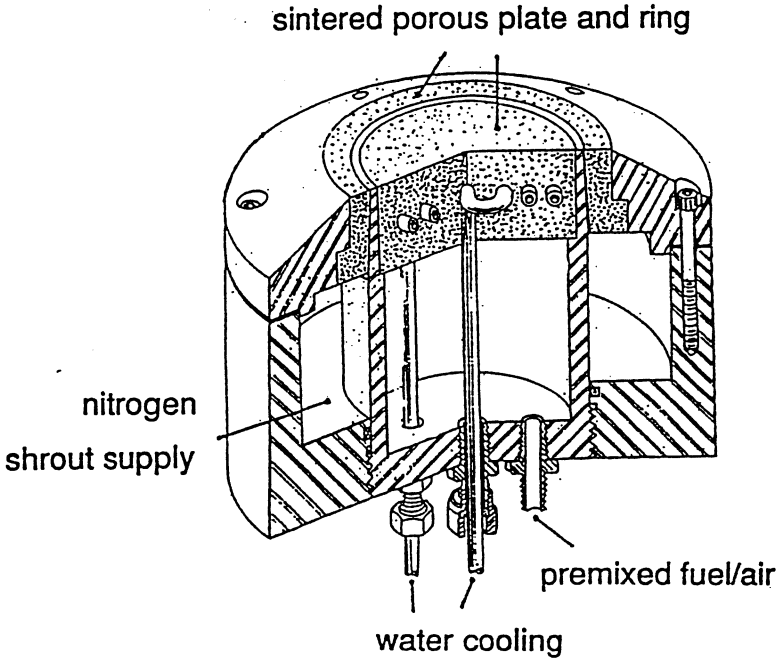

Fig 38: Flat flame burner (McKenna)

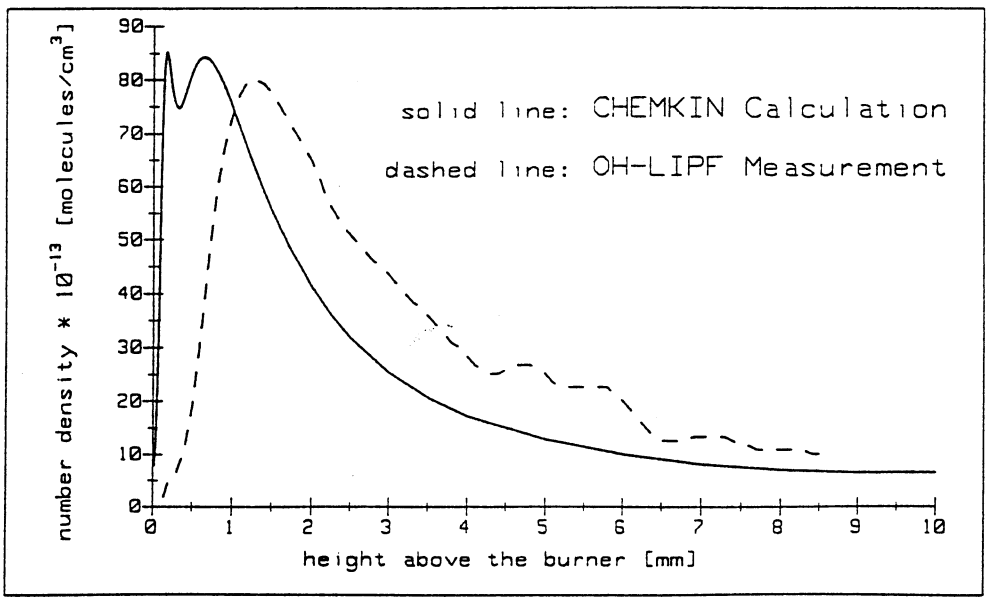

Fig 39: Calculated (CHEMKIN / PREMIX) OH number density versus height above the burner plate. Measured (OH-LIPF) signal versus height above the burner plate

Since the LIPF signal is proportional to the number density of the OH molecules the calculated concentration in a height of 8 mm is used to estimate C and to convert the measured signal intensities to absolute density values.

Temperature Measurement As outlined in Chapter 6.1 the two line approach follows the idea to compare the population densities of two singular quantum states and to calculate the temperature from the density ratio via the Boltzmann equation. Consequently to calibrate the measurement and to determine C from equation 56 line ratios at known temperatures have to be measured in a reference object. The temperature of this facility should be adjustable and cover the expected temperature range of the object under investigation. For this purpose we once again use the hot fan, the heatable cell (600 K to 1100 K) and the flat flame burner (1200 K to 2000 K) described in the previous section. To get the line ratios precisly we record excitation spectra as shown in figure 40.

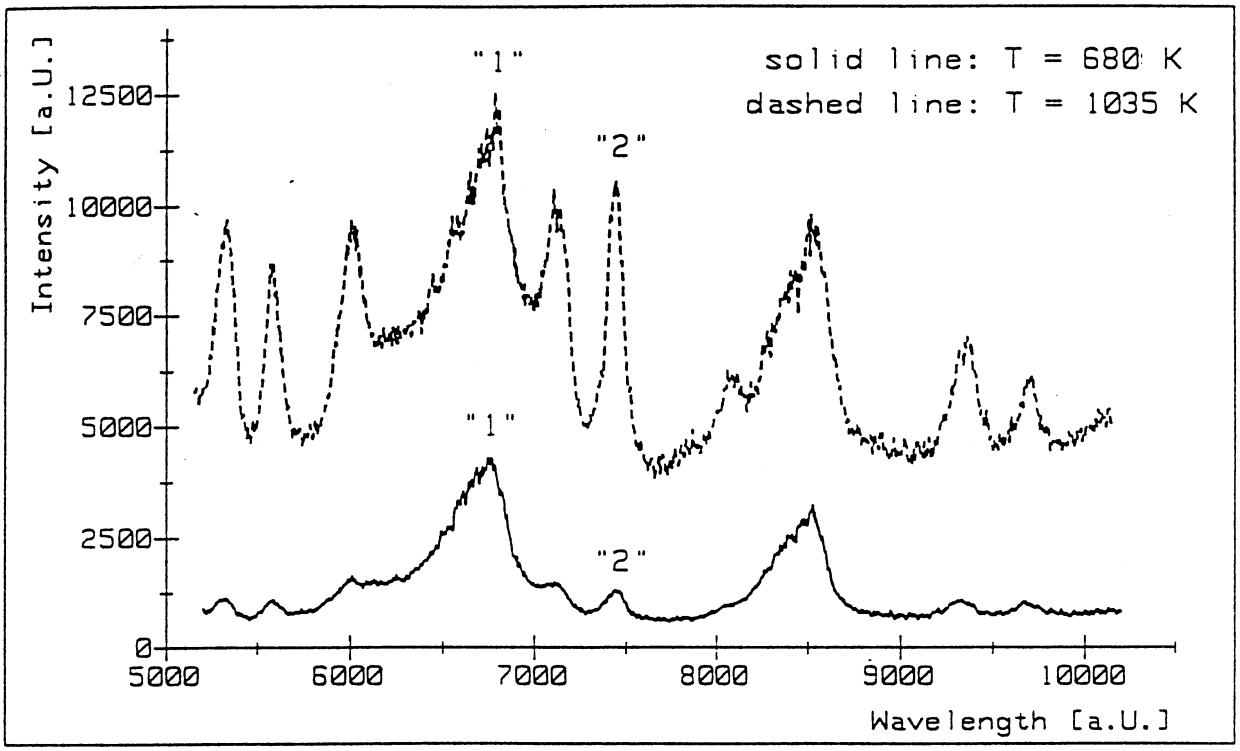

Fig 40: Excitation spectra of hot oxygen (ArF laser at 193 nm, B ← X system) at different temperatures in a heatable cell at atmospheric pressure

In consequence the frequency of the laser is tuned continuosly and the corresponding fluorescence emissions are recorded. It can clearly be seen that the ratio between the marked lines "1" and "2" changes by about a factor of 4 within a temperature range of 600 K to 1100 K. The constant C is calculated from equation 56 for each temperature from the line ratios. The constants are used to calculate an averaged calibration constant $\bar{C}$ which is used in the subsequent measurement of the object under investigation. To cover a temperature range from 300 K to 2000 K different line pairs have to be choosen to probe quantum states that are sufficiently populated to get a high sensitivity and good signal to noise ratios.

6.3. Experimental Setup And Examples Of Applications

Experimental Setup Figure 41 shows a typical setup for planar LIF measurements. The laser beam is formed into a thin light sheet by a set of lenses . The lenses would typically consist of a spherical convex

lens with a long focal length followed by two cylindrical lenses making up a one-dimensional telescope . The achievable size of the light sheet entering the observation volume, especially the maximum height, depends strongly on the effective absorption cross section of the LIF process. The effective cross section again depends on the species undergoing the induced fluorescence process, the selected transition and the chosen technique (linear , saturated or predissociated fluorescence). As a guideline a value of 50 mm may serve for both the height of the light sheet and the width of the observed area, which depends on the angle of divergence of the light sheet and the camera used for observation having a fixed side-length ratio. The typical thickness of the sheet, determining the spatial resolution in this direction, is of the order of 100 μm. In order to suppress background light the beam is trapped in a light absorber after it passed the observation volume.

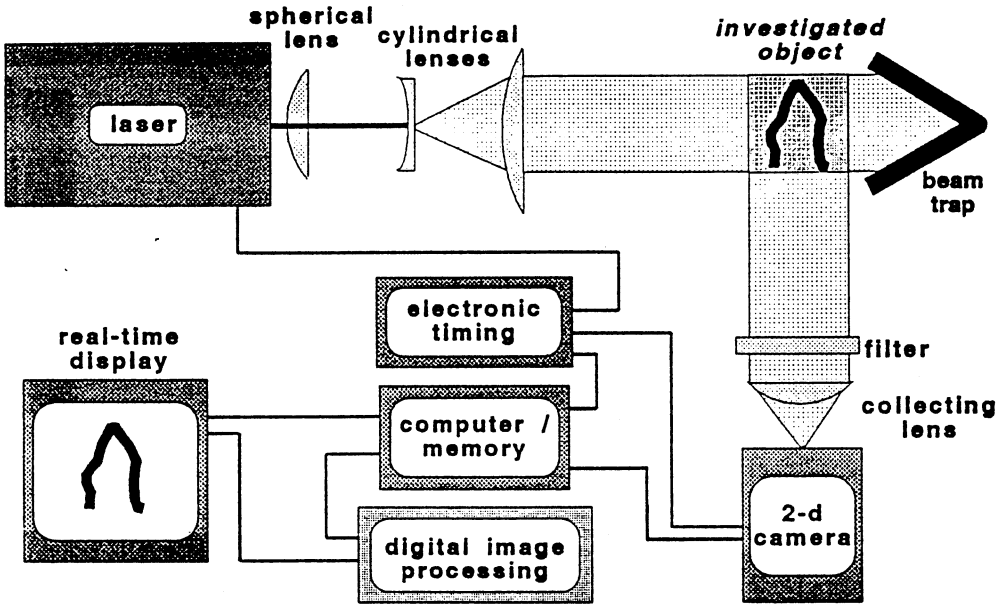

Fig 41: Typical setup for planar laser induced fluorescence measurements. The laser beam is formed into a thin light sheet by means of a long focal length spherical lens and a pair of cylindrical lenses acting as a telescope. The emitted light is captured by collection optics and imaged onto the surface of a solid state detector. In order to limit the light captured by the camera to the desired fluorescence signal, optical filters are used. The data obtained by the detector are transferred to the acquisition and control unit, where they are processed and stored. The control unit is also responsible for the timing requirements of the laser, the camera and, if required, also the experimental system under investigation.

The fluorescence is captured by a collecting lens and imaged onto the detector surface. In the collection path combinations of interference and cut-off filters are positioned, so only the fluorescence signal is actually observed by the detector. The detector is generally a solid-state camera equipped with a gateable image intensifier . The intensity data of the two-dimensional image is transferred from the camera to the acquisition and control unit installed in or coupled with a computer. This control unit is also responsible for the timing of the laser, the camera and the experiment under investigation. The data of the images are stored in grey scale values according to the dynamic range of the camera and the intensity of the emitted light. These digital values can be processed by standard or custom designed procedures for evaluation of concentration and temperature fields. In order to show fine intensity differences the processed image is finally displayed in false colour pictures , where a certain colour is associated with a distinct intensity range.

LIF measurements are not always performed as two-dimensional imaging experiments, but may as well

be integrated in other spectroscopic techniques . In this case the setup is different from the one shown above, but rather looks similar to the setup for Rayleigh and Raman scattering (see Chapter 6). The application of LIF in a "spectroscopical setup" will be shown in one of the examples below.

LIF applications in combustion processes require tunable , intense, pulsed lasers in the deep UV. Tunability is required because of the resonant nature of the excitation process. The intensity is required for high excitation efficiency, which is the origin for the high sensitivity of LIF. The lasers have to be pulsed to distinguish the laser induced emission from the emission arising naturally in combustion: with short pulsed lasers, in combination with gated fluorescence detection, the natural emission is suppressed by orders of magnitude. The operation in the deep UV is required because the spectroscopy of combustion species is almost exclusively in this frequency range .

In most LIF applications Nd-YAG or excimer lasers are used to pump tunable dye lasers in the visible part of the spectrum. Frequency doubling or mixing is typically used to generate the desired frequencies in the deep UV. Pulse durations of such laser systems are in the range of 10 ns. Bandwidths in the UV around 0.2 cm^{-1} are relatively easy to achieve. Most LIF applications a few years ago were performed with rather moderate pulse energies of μJ to a few mJ at maximum. Since the invention of BBO crystals , the pulse energies available in the deep UV (210 - 250 nm) became much higher (several mJ per pulse), which in many cases is sufficient for planar LIF imaging on considerably large laser sheets.

An alternative to such fully tunable deep UV lasers are tunable excimer lasers . These lasers have the highest spectral brightness and pulse energies in the deep UV (a few 100 mJ per pulse within less than a wave number). Although they operate only in a narrow frequency range (KrF: 193 - 194 nm, ArF: 248 - 249 nm) a variety of different LIF techniques can be used to detect important combustion species (like OH, O_2, H_2O, NO, CO). Additionally these lasers offer more advantages for laser diagnostics . They are easily frequency shifted by stimulated Raman scattering in high pressure hydrogen cells, opening up other tuning ranges . Because of their deep UV wavelength, "tracer molecules" , added to the flow for visualization purposes or to hydrocarbon fuels to measure fuel air ratios can be excited efficiently. The lasers can also be used - with slight modifications - to pump dye lasers and generate fully tunable UV radiation. In addition, due to their extreme power in the deep UV, the lasers are ideally suited for "normal" Rayleigh and Raman diagnostics . In this way many different laser diagnostic techniques can be employed with just tunable excimer lasers . The lack of full tunability is nevertheless a considerable disadvantage in a number of applications.

On the detection side, only a few years ago, photomultipliers had been used almost exclusively for the detection of fluorescence. Today, modern camera technology has greatly increased the potential of LIF methods. The development of short gated photometric camera systems with ultimate sensitivity (matching that of phototubes), in combination with powerful digital image processing opens up new areas for LIF applications. It has been mentioned that cameras in combination with laser sheets are used for two-dimensional laser induced fluorescence imaging from spatially well defined planes and that spatial scanning in the third dimension will yield species and temperature distributions in all three dimensions. In the example discussed below, it is demonstrated that even qualitative information from such images allows details about mixing and combustion to be understood.

One other important design consideration in imaging experiments is the choice of the lens projecting the image on the photo-sensitive surface. LIF diagnostics in combustion is almost always done in the deep UV. The only commercially available lens for this region of the spectrum is the UV-Nikkor from Nikon. Although this lens features excellent characteristics with high spatial resolution, it is not designed for weak light collection, i.e. it shows poor collection efficiency . Despite the fact that LIF is famous for its high sensitivity, the accuracy of LIF measurements depends crucially on the light collection efficiency. At the cost of some spatial resolution , the collection efficiency can be increased easily by a factor of 10 with specially designed UV lens combinations with a spatial resolution still below 100 μm. Since this resolution is of the same order as the resolution given by the thickness of the laser sheet , it represents no real deficiency. The use of a carefully selected imaging lens is therefore by far the most inexpensive

way to improve the measurement precision.

Examples of Applications Because of its great selectivity and sensitivity, the method of Laser Induced Fluorescence has been used to investigate the flame structure and to detect the important minory species in complex combustion processes. The first example refers to unstationary combustion of H_2 in air. The experimental setup consists of a tube with a length of 0.5 m and a rectangular crosssection of 60 x 30 mm (see Fig. 42). To obtain different turbulence intensities the main flow velocity was varied and different obstacles were mounted in the tube. The initial concentration of hydrogen was varied in a lean mixture range from 10 to 20 Vol-% in order to change the effective turbulent burning velocity, which is proportional to the laminar burning velocity and therefore directly correlated with the concentration. As an interim reaction product the OH-radicals indicating the reaction zones were excited with a pulsed Excimer laser (XeCl, 308 nm) causing Laser induced Fluorescence. Therefore the longitudinal section of the flame could be visualized with a thin light sheet. Fig. 43 shows the optical setup and a LIF recording of a flame front.

Limitations of LIPF Despite the advantages of LIPF discussed in Section 6.1, great care has to be taken in the application of this technique to avoid the problems mentioned in the following section.
First, collisions become important again if the pressure increases. With rising pressure the quench rate increases and becomes, at certain pressures, as large as the predissociation rate. This implies that LIPF works quantitatively only up to a certain pressure limit, which is roughly reached when the quench rate Q equals the predissociation rate P. For example in the case of the detection of the OH radical Schwarzwald et al. Schwarzwald, [1987] and Köllner et al. Köllner, [1990] showed that collisions reduce the actual lifetimes τ_0 and τ_1 of the excited states v'= 0 and 1 in the burned gases of a hydrocarbon-air flame at atmospheric pressure to about 2 ns. The corresponding predissociative lifetime τ_3 of the v'= 3 level at the same flame conditions is about 0.1 ns (Gray, [1992]). As an approximation it can be assumed that v'= 0, 1, 2 and v'= 3 have the same quenching cross section. A comparison of τ_3 with $\tau_{0,1}$ shows that only 5 % of the OH radicals with v'= 3 are quenched at atmospheric pressure during their lifetime when using this predissociative upper energy level. At 20 bars, however, the collision quenching lifetime of the v'= 3 state would be 0.1 ns, which is roughly equal to the pressure independent predissociative lifetime τ_3. Since the loss rate is the same for quenching and predissociation, about 50 % of the signal would need correction. As said in the previous sections this correction is often not possible because of the unknown quenching conditions (T, p, xi). Therefore a quantitative application of the LIPF technique for the detection of OH at pressures higher than 20 bars is not possible. It should be mentioned that the pressure limit for quantitative measurements with LIPF strongly depends on the molecule under investigation because the predissociative lifetime is a molecular constant (e.g. τ_{O2} (v'=10) $\approx$ 6 ps (Kim, [1991]).

A second problem is caused by the depletion of the probed ground state at high laser power. The depleted state may be refilled from other quantum states by collisions in the ground state during the laser pulse and the molecules can be excited again by the laser. This increases the fluorescence intensity artificially and makes the LIPF signal again dependent on the collisional environment. Therefore the rotational and vibrational energy transfer (RET and VET) in the ground state has to be strictly avoided. This can be done by using moderate laser fluxes which keep the excitation efficiency well below 20-30 %. The loss of detection sensitivity which is caused by this strategy can be partially compensated by averaging or by better collection optics.

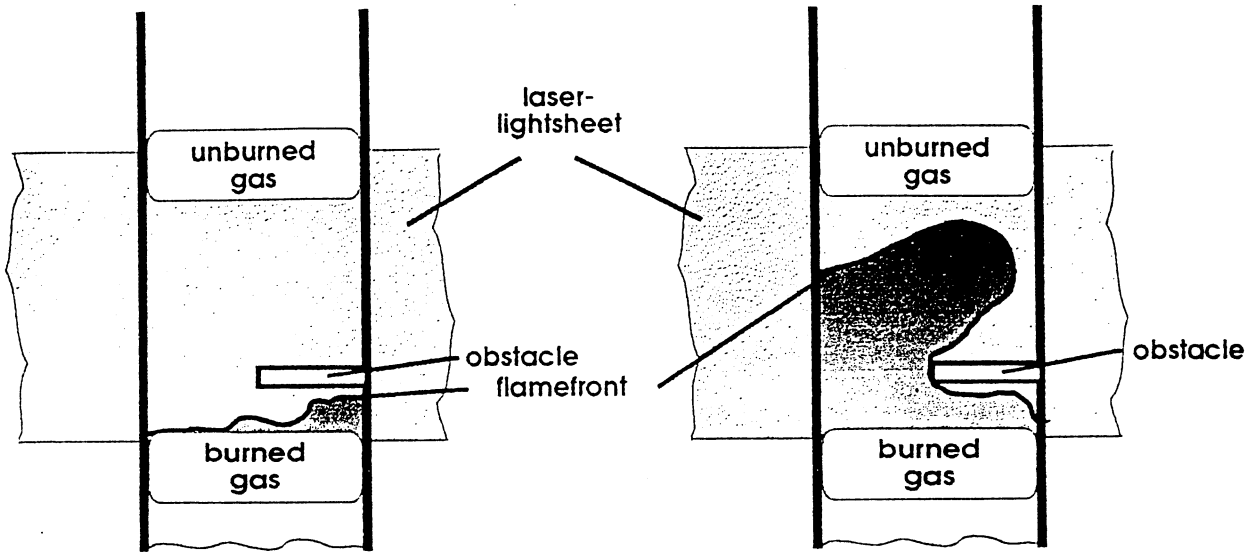

Fig 42: Unstationary burner with mounted obstacles in the tube

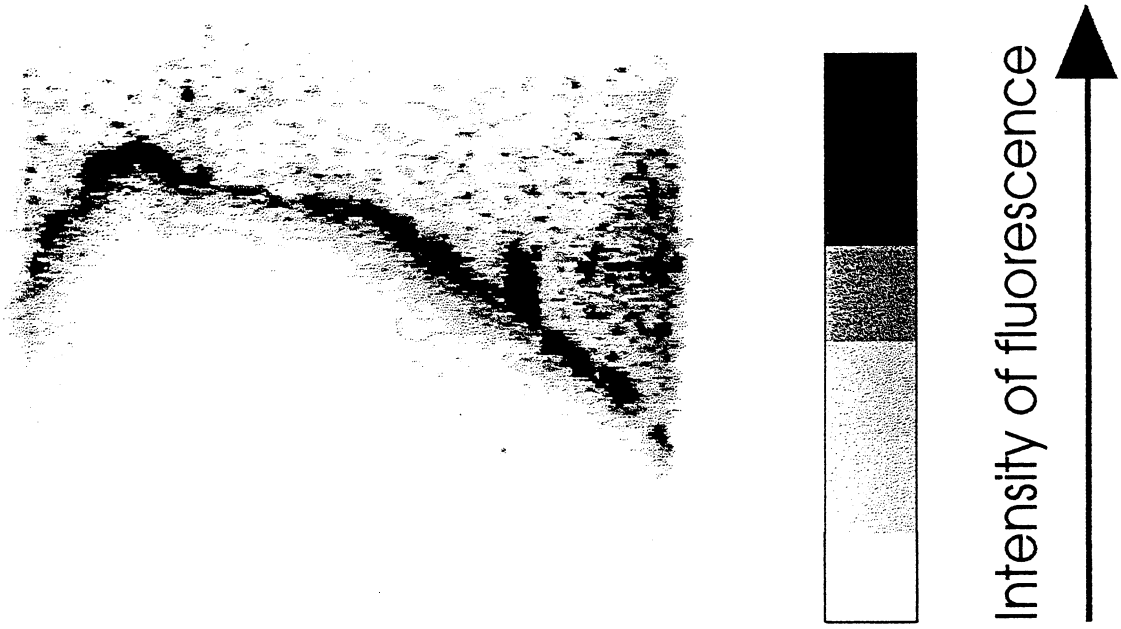

Fig 43: LIF recording of a flame front

Another important aspect for the quantitative application of LIPF is the rotational and vibrational energy transfer (RET and VET) within the excited state. The RET/VET process may lead to fluorescence light from states with much longer predissociation lifetimes. The emission from these states (so called indirect fluorescence) is collisionally affected and has to be suppressed. This can be done by suitable filters (e.g. dielectric mirrors). For example in the case of the OH detection ($A^2\sum^+, v' = 3 \leftarrow X^2\Pi, v'' = 0$ excitation) only the single lines of the 3 → 2 band should be detected, because the 2 → 2, 2 → 1, 1 → 1, 1 → 0 and 0 → 0 transitions are strongly affected by collisions with other species in the flame. This phenomena is illustrated in Figure 44 showing broad and less structured emissions from the lower vibrational states indicating population in many rotational states by direct vibrational quenching or from rotational energy transfer in these levels.

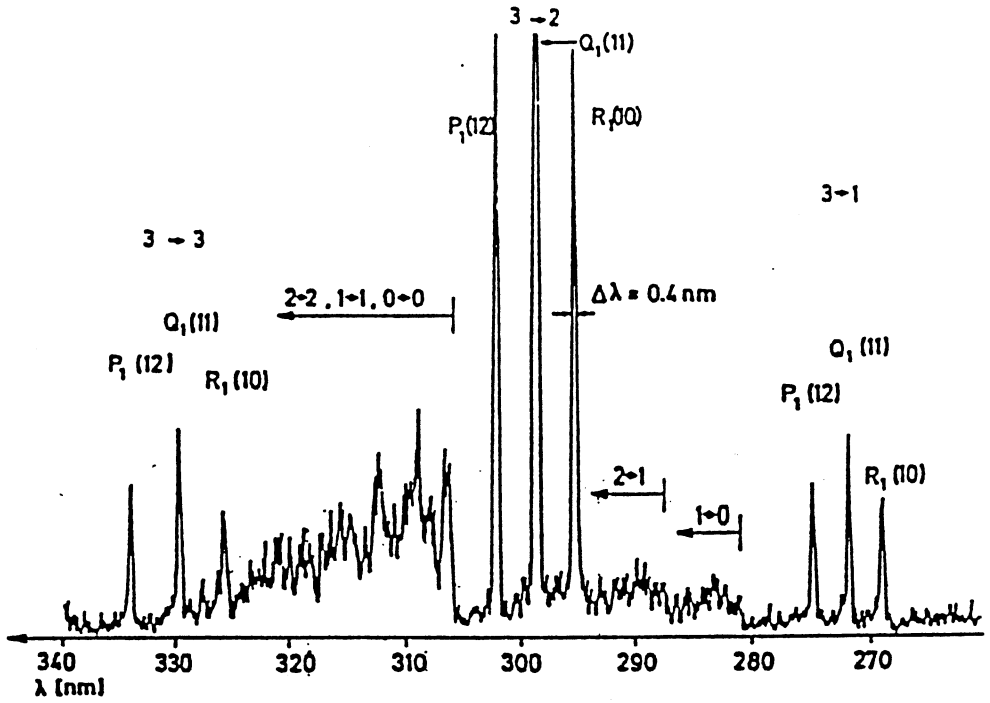

Fig 44: OH dispersion spectrum for a butane flame. OH is excited on the Q_1 (11) line. The spectral resolution is $\approx$ 0.4 nm. The spectral range of different vibrational bands for the OH($^2\sum - ^2\Pi$) transition is indicated. The Q1 (11) and P1 (12) lines are off scale (Andresen, [1988]).

Implicit in the development of laser diagnostics is the assumption that the laser radiation has no perturbing effect on the parameters being measured. There may however be cases where the laser does perturb local combustion parameters such as temperature, since the absorption of laser radiation acts as an energy input mechanism, or the chemical structure, through the photo-production of radicals. In LIF measurements of O atoms in flames, Miziolek and DeWilde (Miziolek, [1984]) found that the laser was significantly altering the O concentration during the measurement, through multiphoton dissociation of fuel and oxidizer. On the other hand Meijer et al. (Meijer, [1986]) showed that the influence of the laser on the chemistry of the molecules must not always be a disadvantage. He reported in his paper that the OH photofragment fluorescence resulting from photodissociation of water vapor can be used to detect the parent molecule.

In addition some more practical limitations of the LIPF technique have to be considered. First, the excitation to predissociative states is only possible if there is a potential crossing in the energy diagramm of the molecule leading to a repulsive state with subsequent dissociation and that this state can be reached by the laser source. Preliminary studies show that O2, OH and H2O can be excited to predissociative states within the tuning range of an ArF (193 nm -194 nm) or a KrF (247 nm - 248 nm) excimer laser. Second, the strong predissociation leads to a great loss of excited molecules and therefore the fluorescence yield, known as the Stern-Vollmer factor F/(F+P+Q), is small. The low signals sometimes require averaging which leads to a loss in space and/or time resolution. Last, if instantaneous temperature fields have to be measured, which is for example necessary for the understanding of the NOx formation in highly turbulent flames, the requested equipment is twice as much as for concentration measurements (two lasers and two

cameras are needed) which cause high equipment costs.

7. Concluding Remarks

Optical measurement techniques are very versatile methods of obtaining species concentrations and temperatures in sub- and supersonic combustors. These techniques are used when measurements with conventional measuring techniques lead to significant influences of the results due to the interaction between the probes and the investigated flowfield.

Non spectroscopic techniques like holographic interferometry allows to investigate on line the mixing process in the combustion chamber. It is also possible to measure the concentration of major species in the mixing area of the ram-combustor without perturbing the flowfield, but with the limitation to 2-dimensional flow structures.

The area in which Raman scattering is currently most widely applied are combustion processes. In these systems the important mixing processes of fuel and oxidizer before the reaction can be investigated as well reaction kinetics in the flame zone and the species contained in the exhaust gases. One major advantage of Raman spectroscopy over other applicable measuring techniques is the possibility of the simultaneous measurement of concentrations of all species involved and of the temperature in the flowfield of the combustion chamber.

The self fluorescence technique allows to investigate the overall structure of sub- and supersonic flames. It is also possible to investigate the fluctuations of highly turbulent flames. In comparison with laser based techniques such as Raman scattering or laser induced fluorescence the accuracy of the obtained data is significantly lower when self fluorescence is employed. In addition, the achievable resolution both in time and spatial is much better in laser based experiments. However, if a combustion system is to be investigated in detail, a very suitable path of investigation is the employment of self fluorescence first in order to capture the general behaviour of the system. Based on these results, laser techniques are subsequently applied only to the main points of interes in the system. This may save not only lots of time that goes along with laser based experiments, but at the time even more costs.

Laser induced fluorescence methods are extremely powerful tools, mainly applied to concentration and species measurements in combustion chambers. The strength of the fluorescence signals is often many orders above that of Raman and Rayleigh scattering techniques, yielding very good signal-to-noise ratios even in planar applications. Even for large areas of observation of several centimeters side length the achievable spatial resolution is very good and the resloution in the third dimension, defined by the thickness of the exciting laser light-sheet, is of the order of 100 μm. Temporal resolution is mainly determined by the excitation source. For pulsed lasers typically used for LIF measurements it is usually in the lower nanosecond range.

One of the most important advantages of LIF - compared to most other laser diagnostic methods - is its extreme selectivity and sensitivity. The extreme selectivity of LIF results from the fact that molecules can be excited resonantly only at very few selected frequencies and that the subsequent emission represents a highly characteristic fingerprint of the emitter. The extreme sensitivity originates from the efficient excitation by pulsed deep UV lasers and the highly sensitive detection of photons. These factors make LIF ideally suitable for the important detection of minority species in complex reaction systems, especially combustion processes. Minority species like OH play a central role in our basic understanding of combustion processes because they represent sensitive probes of the detailed reaction dynamics and indicate, for example, the positions of flame fronts. Most pollutants like NO, NO_2 or CO are minority species that can only be detected by LIF. Although LIF can basically also be used for the detection of

majority species as well (e.g. O_2, H_2O), its main domain is the detection of minority species. It allows one to selectively probe even single quantum states of molecules, e.g. in real internal combustion engines, which is difficult with any other laser diagnostic method.

References

M. Alonso, E.J. Finn; 'Quantum Physics', Edison-Wesley; 1988.

P.Andresen, A.Bath, W.Gröger, H.W.Lülf, G.Meijer, J.J.ter Meulen, 'Laser-induced fluorescence with tunable excimer lasers as a possible method for instantaneous temperature field measurements at high pressures: check with an atmospheric flame'; Appl. Optics 27/2, 365 (1988).

U. Brackmann; 'Lambdachrome Laser Dyes'; Lambda Physik, Göttingen 1986.

W. Demtröder; 'Laserspektroskopie', Springer-Verlag, 1991.

G.H. Dieke, H.M.Crosswhite;'The Ultraviolet Band of OH', J Quant. Spectrosc. Radiat. Transver, Vol2; 1962.

A.C. Eckbreth, P.A.Bonczyk, J.F. Verdieck; 'Combustion Diagnostics by Laser Raman and Fluorescence Techniques', Prog. Energy Comb. Sci, Vol 5; 1979.

N. Everall, R. W. Jackson, J. Howard, K. Hutchinson; 'Fluorescence Rejection in Raman Spectroscopy Using a Gated Intensified Diode-Array-Detector', Journal of Raman Spectroscopy, Vol 17, pp. 415-423.

A.G. Gaydon; 'The Spectroscopy of Flames', Chapman and Hall, London 1974.

R. Goulard; 'Combustion Measurements', Hemisphere Publishing Corp., 1976.

J.A.Gray, R.L.Farrow, 'Predissociation lifetimes of OH A 2S+ (vÆ=3) obtained from optical-optical double-resonance linewidth measurements', J. Chem. Phys., Vol.95(10), pp.7054-7060 (1992)

R.K. Hanson, J.M. Seitzmann, P.H. Paul; 'Planar Fluorescence Imaging of Gases', Applied Physics, Vol.B 50 1990.

R.K. Hanson; 'Combustion Diagnostics: Planar Imaging Techniques', 18th Symp. (Intl.) on combustion, The Combustion Institute; Philadelphia, PA, 1986.

M. Haibel, F. Mayinger; 'Turbulence induced mixing and stabilization of sub- and supersonic hydrogen-air-flames', Conference of the DGLR in Bremen, FRG; 1992.

M. Haibel, F. Mayinger, G. Strube; 'Application of non-instrusive diagnostic methods to sub- and supersonic H_2-air-flames', Non-Intrusive diagnostic Conference in Scheweningen (Den Haag), 1992.

W. Hauf, U. Grigull; 'Optical Methods in Heat Transfer', Advances in Heat Transfer 6, 1970.

G. Herzberg; 'Molecular Spectra and Molecular Structure', I. Spectra of Diatomic Molecules; van Nostrand, New York 1966.

K.P. Huber, G. Herzberg;'Constants of Diatomic Molecules'; van Nostrand, New York, 1979.

R.J.Kee, J.A.Miller, T.H.Jefferson, 'CHEMKIN, a general purpose, problem independent transportable, Fortran chemical kinetics code package', Sandia Laboratories report, Sand 80-8003 (1980)

R.J.Kee, J.Warnatz, J.A., 'A Fortran computer code package for the evaluation of gasphase viscosities, conductivities, and diffusion coefficients', Sandia Laboratories report, Sand 83-8309 (1983)

R.J.Kee, J.F.Grear, M.D.Smooke, J.A.Miller, 'A Fortran program for modeling steady laminar one-dimensional premixed flames', Sandia Laboratories report, Sand 85-8240 (1985)

R.J.Kee, F.M.Rupley, J.A.Miller, 'CHEMKIN thermodynamic data base', Sandia Laboratories report, Sand 87-8215 (1987)

G.S.Kim, L.M.Hitchcock, E.W.Rothe, G.P.Reck, 'Identification and Imaging of hot O_2 (v" = 2,3, or 4) in hydrogen flames using 193 nm- and 210 nm-range light', Appl. Phys. B 53, 180 - 186 (1991)

M.Köllner, P.Monkhouse, J.Wolfrum, 'Time-resolved LIF of OH ($A^2\sum^+, v' = 1 and v' = 0$) in atmospheric-pressure flames using picosecond excitation', Chem. Phys. Letters , Vol.168, 3/4, pp.355-360 (1990)

Landolt-Börnstein; Berlin, 1982.

M. Lapp, D.L. Hartley; 'Raman Scattering Studies of Combustion', Combustion Science and Technology, Vol 13, pp. 199-210.; 1976.

N.M. Laurendeau; 'Temperature Measurements by Light-Scattering Methods', Prog. Energy Combust. Sci., Vol 14, pp. 147-170.

S. Ledermann; 'The Use of Laser Raman Diagnostics in Flow Fields and Combustion', Prog. Energy Combust. Sci, Vol.3, pp.1-34; 1980.

A. Leipertz; 'Laser-Raman-Spektroskopy in der Wärme und Strömungstechnik',Physik in unserer Zeit, Vol. 4, pp. 107-115 1981.

F. Mayinger, W. Panknin;'Holography in heat and mass transfer', Proc. 5th Int. Heat Transfer Conference, Tokyo, Vol. 6, 28-43. 1974.

F. Mayinger;' Optical Measurement Techniques', Springer Berlin 1993.

G.Meijer, J.J.ter Meulen, P.Andresen, A.Bath, 'Sensitive quantum state selective detection of H_2O and D_2O by (2+1)-resonance enhanced multiphoton ionization', J. Chem. Phys. ,Vol.85(12), pp.6914-6922 (1986)

A.W.Miziolek, M.A. DeWilde, 'Multiphoton photochemical and collisional effects during oxygen-atom flame detection', Opt. Letters,Vol. 9(9), pp. 390-392 (1984)

S. Neti, C. Anastaia, W. Smith, J. C. Chen; 'Ramanscattering in Two Phase Flows with Application to Temperature Measurements', in Measuring Techniques in Gas-Liquid Two-Phase Flows, Springer 1984, Berlin.

D.A. Long; 'Raman Spectroscopy', McGraw-Hill, London 1977.

W. Panknin; 'Eine holographische Zweiwellenlängeninterferometrie zur Messung überlagerter Temperatur- und Konzentrationsgrenzschichten.', Dissertation, T.U. Hanover 1977.

S. S. Penner, C. P. Wang, M. Y. Bahadori; ' Laser Diagnostics applied to Combustion Systems.', 20th Symposium (International) on Combustion, pp. 1149-1176, Combustion Institute, 1984.

B. Ruck; ' Lasermethoden in der Strömungsmesstechnik.'AT Verlag, Stuttgart, 1990.

G. Strube, F. Mayinger; 'Struktur und Brenngeschwindigkeit von hochturbulenten Wasserstoff-Luft-Flammen' BMFT 1500769.

R.Schwarzwald, P.Monkhouse, J.Wolfrum, 'Picosecond fluorescence lifetime measurements of the OH radical in an atmospheric pressure flame', Chem. Phys. Letters , Vol.142, 1/2, pp.15-18 (1987)